SC/68A/SH/12

Linking climate and ocean productivity to the prevalence of southern right whales (Eubalaena australis) in South African waters

Gideon van den Berg, Els Vermeulen, Cang Hui, Ken Findlay, Sophie von der Heyden and Guy Midgley

INTERNATIONAL WHALING COMMISSION

Linking climate and ocean productivity to the prevalence of southern right whales (*Eubalaena australis*) in South African waters

Gideon van den Berg[1], Els Vermeulen[1], Cang Hui[3], Ken Findlay[4], Sophie von der Heyden[2], Guy Midgley[2]

1. Mammal Research Institute Whale Unit, Department of Zoology and Entomology, University of Pretoria, Lynnwood Rd, Hatfield, Pretoria 0002, South Africa
2. Department of Botany and Zoology, Stellenbosch University, Matieland 7602, South Africa
3. Department of Mathematical Science, Stellenbosch University, Matieland 7602, South Africa
4. Oceans Economy, Cape Peninsula University of Technology, Keizersgracht St, Zonnebloem, Cape Town 7925, South Africa

Abstract

South African coastline surveys conducted since 1972 reveal fluctuations and a recent reversal in a long-running increasing trend in regional abundance of southern right whales (*Eubalaena australis*, hereafter SRWs), whose populations have been recovering from historic whaling. Furthermore, the surveys reveal that the typical three-year calving cycle of female SRWs has shifted to four- or five years, implying either additional resting years between successive calving events or calving failure. This study used wavelet analysis, an effective method of time series analyses on non-stationary data, to reveal significant synchrony in the cycles of SRW cow-calf pair annual counts along the South African coast and various climate indices (Oceanic Niño Index, September Antarctic sea ice extent and the Antarctic Oscillation) as well as ocean colour (January chlorophyll *a* concentrations in three postulated SRW feeding grounds). In addition, autoregressive integrated moving average (ARIMA) models were used to investigate the potential role played by ocean colour and the various climate indices in the inter-annual fluctuations of cow-calf pair counts, as well as the recent reversal in the increasing trend of regional abundance. The impacts of climate are thought to be mediated through the influence of physical oceanography on SRW prey (krill and copepod) availability, while chlorophyll *a* concentrations have been found to correlate with densities of SRW prey. These aspects ultimately impact feeding success and body condition of SRWs, and consequently their reproductive condition and migratory behaviour. ARIMA models analysing the recent reversal in the increasing trend of abundance in SRW cow-calf pair counts along the coast of South Africa, reveal significant model performance improvement through the inclusion of the Oceanic Niño Index, the Antarctic Oscillation and chlorophyll *a* concentration data from one of the three postulated SRW feeding grounds. Results of this study indicate that SRW calf abundance in coastal South Africa appear closely influenced by the species' life cycle, as well as feeding ground productivity and global climate indices, similar to findings for other SRW populations.

Introduction

Southern right whales (*Eubalaena australis*, hereafter SRWs) are baleen whales which range between 20° and 60°S where they feed on plankton, primarily Antarctic krill (*Euphausia superba;* hereafter krill) and copepods (NMFS 2007, Nicol et al. 2008, Reilly et al. 2013). Being once very abundant, SRWs were strongly reduced in numbers by the open-boat whaling industry, which in Southern Africa began in the late 1700s. Only in 1935 did the species become internationally protected, when fewer than 1% of their original numbers remained (IWC 2013). This protection has allowed breeding populations of SRWs in South Africa to increase by as much as 7.1% per year (Best et al. 2001). However, the annual abundance of SRWs along the South African coastline has recently shown evidence of returning to a decline between 2015 and 2017, after rising for more than three decades (*Figure 1*). Interestingly, in 2018, counts of SRW cow-calf pairs increased substantially, while the counts of unaccompanied adults (males and non-calving females) remained low. In conjunction with these fluctuating trends of abundance, many female SRW calving intervals have shifted from a three-year reproductive cycle to a four- or five-year cycle (Brandão et al. 2018, Vermeulen et al. 2018).

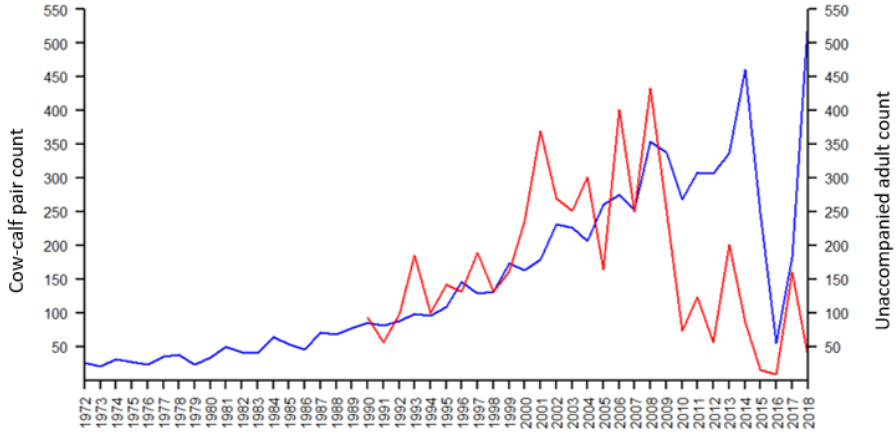

Figure 1. Field counts of southern right whales observed during annual aerial surveys between Nature's Valley and Muizenberg, South Africa, between 1972 and 2018 (MRI unpublished data). Blue line indicates cow-calf pair counts (1972 – 2018); red line indicates unaccompanied adult counts (1990 – 2018).

Female SRWs normally calve approximately every three years (Best & Folkens 2007, Brandão et al. 2011). Pregnancy and lactation in SRW females are energetically demanding and the reproductive output of this species has been found to respond to fluctuations in krill abundance in other breeding grounds (Leaper et al. 2006, Seyboth et al. 2016). In fact, several studies have shown suppressed reproduction in cetaceans during periods of nutritional stress (Lockyer 1986, Reeves et al. 2000, Greene et al. 2003, Hlista et al. 2009, Ward et al. 2009, Williams et al. 2013). The connection between nutrition and the reproductive output of SRWs is found in their body condition (i.e. their blubber thickness). Evidence of the existence of prey limited reproduction suggests that the increasing calving intervals seen in South African SRWs, as well as the recent large shifts in the annual abundance of SRWs in the South African breeding ground, could potentially be linked to changes in prey availability and therefore productivity in SRW feeding grounds. This knowledge, combined with the known site fidelity of SRW to breeding and feeding grounds (Patenaude et al. 2007, Valenzuela et al. 2008, 2009, Carroll et

al. 2015) should allow causal links to be made between the conditions of specific feeding regions and observed reproductive success.

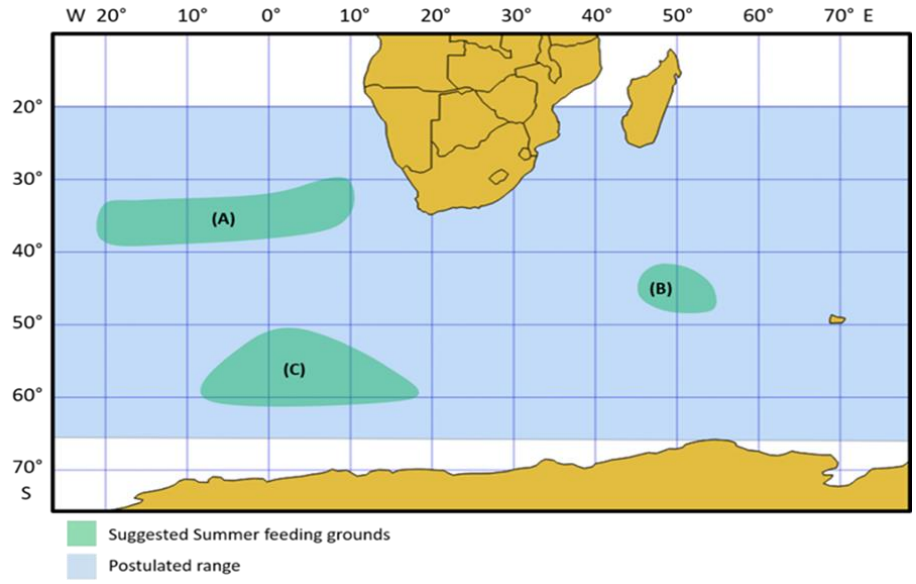

Figure 2. Summer feeding grounds (illustrated via A, B and C) of the South African population of SRW as suggested by Best and Folkens (2007). Feeding ground A: a section of the southern Atlantic Ocean between 30°S and 40°S. Feeding ground B: a section of the southern Indian Ocean between 40°S and 50°S around the Crozet islands. Feeding ground C: a section of Southern Ocean between 50°S and 60°S.

The South African SRW population is thought to have at least three wide-ranging summer feeding areas in the Southern Ocean (see *Figure 2*). It must be noted however, that the locations of these feeding grounds are based largely on illegal Soviet catch data (Tormosov et al. 1998) and Townsend's (1935) charts of open boat whaling catches, and are therefore not directly confirmed (Best & Folkens 2007). In general, relatively little is known about the diet of South Africa's SRWs (Best & Folkens 2007). However, the stomach contents of 249 illegal SRW catches in the 1960s showed that 99.4% of SRW samples taken south of 50°S had stomach contents containing krill. In contrast, 91.7% of samples taken north of 40°S contained copepods. Between 40° and 50°S, SRWs were shown to be feeding on copepods (71.4%), krill (24.3%), or other 'small crustacea' (4.3%) (Tormosov et al. 1998). Stable isotope analysis on 11 SRWs sampled in South Africa revealed strong seasonality in their feeding, with feeding dropping off after May and resuming again in August to December (Best & Schell 1996).

Both breeding and survival success of many species in the Southern Ocean, including SRWs, have been found to be influenced by krill abundance (Croxall et al. 1999, Fraser & Hofmann 2003, Forcada et al. 2005, Leaper et al. 2006, Trathan et al. 2007, Jenouvrier et al. 2009, Trathan et al. 2011, Barbosa et al. 2012, Seyboth et al. 2016). Importantly in the context of this study, strong correlations have been found between the breeding success of SRWs in Argentina and Brazil with krill abundance in their summer feeding ground off South Georgia (Leaper et al. 2006, Seyboth et al. 2016). Krill abundance in South Georgia was found to be driven by SST anomalies and global climate indices such as the El Niño-Southern Oscillation (ENSO) and the Antarctic Oscillation (AAO)

(Trathan et al. 2003, Leaper et al. 2006, Seyboth et al. 2016). Seyboth et al. (2016) suggests that an increased frequency of years with low krill abundance, potentially due to changing marine environments, is likely to have adverse impacts on the rebounding SRW populations in the Southern Hemisphere. Baleen whale responses to climate change, however, need to be interpreted with caution, since responses are confounded by the fact that virtually all populations are recovering from overexploitation (Nicol et al. 2008).

Using a time series analyses approach, this study aims to test for possible links between climatic, oceanic and biological factors and the inter-annual fluctuations and longer-term changes in SRW prevalence on the southern African coastline. Notably, the term 'climate variability' includes both natural variability and possible anthropogenic climate change, whose impacts on SRWs are putatively mediated through the influence of physical oceanography on plankton (specifically copepods and krill). These impacts are thought to influence the body condition of SRWs and thus their reproductive output and migratory behaviour (see Greene & Pershing 2004). More specifically, this study investigates the influence of chlorophyll *a* concentrations in three postulated summer feeding grounds (*Figure 2*), as well as relevant climatic factors that may influence SRW food availability via effects on physical oceanography.

Materials and Methods

Photo-ID data collection

Aerial surveys of SRWs have been conducted annually in October since 1972, with a photo-identification component since 1979, between Muizenberg (34°07'29"S 18°29'09"E) and Nature's Valley (33°59'49"S 23°33'40" E), South Africa. For detailed methodology, see document SC/68A/SH/01. From these surveys, count data of cow-calf pairs (1972-2018) and unaccompanied adults (1990-2018) were obtained for use in this study. Given that the count data of SRW unaccompanied whales are substantially shorter in length compared to the cow-calf pair data (*Figure 1*), all time-series data analyses were performed on the SRW cow-calf pair count data alone. It needs to be noted that these data refer to counts and not uniquely identified individuals, meaning that duplicates may be present within the count data. However, the number of duplicate counts in one given year (when comparing count data with the number of uniquely identified individuals) remains relatively stable over the survey series, averaging 17%.

Climate indices

The potential effects of climate on South African SRW counts were investigated using data from various climate indices. The El Niño–Southern Oscillation (ENSO), which identifies sea-surface temperature (SST) variability in the eastern Pacific Ocean and air surface pressure variability in the western Pacific, has been found to drive inter-annual cycles of sea ice extent around Antarctica (Loeb et al. 2009, Loeb & Santora 2015), which is known to influence krill densities (larger winter sea ice extent, more krill) (Loeb et al. 1997, Fraser & Hofmann 2003, Atkinson et al. 2004, Flores et al. 2012, Trathan et al. 2012). ENSO fluctuates between two phases, El Niño and La Niña, which disrupt the typical Pacific oceanic and atmospheric circulations (Salinger et al. 2016). The Niño 3.4 Index is one of the primary measures of oceanic variation associated with warm El Niño and cold La Niña

periods. As such, the Oceanic Niño Index (ONI; the 3-month running mean of the Niño 3.4 Index) was included in the analyses. The Antarctic Oscillation (AAO), otherwise known as the Southern Annular Mode, is the leading mode of atmospheric variability south of 20°S (Pohl et al. 2010, Salinger et al. 2016). The AAO describes the north–south movement of the westerly wind belt that encircles Antarctica. A positive AAO phase is characterized by the southward shift of the wind belt together with an increased intensity in the winds (Loeb & Santora 2015). Over the past 30 years, an increase in the positive phase of the AAO has been noted, which has been partly attributed to increased westerly winds resulting from Antarctic ozone depletion (Cai 2006, Flores et al. 2012). The increase in the AAO has resulted in increased poleward heat transport and the southward shift of fronts in the ACC, which is suggested to have positive and negative impacts on Antarctic ecosystems (Flores et al. 2012). As such, the AAO was also included in the analyses. Climate indices were obtained from the database available on the NOAA Climate Predict Center (http://www.cpc.ncep.noaa.gov/). Yearly means of the climate indices were obtained in the same way as done in a number of other studies dealing with teleconnections, whereby the data were averaged from June of the previous year to May of the year being considered (Liu et al. 2002, Leaper et al. 2006, Seyboth et al. 2016). Given the tight association between krill and winter sea ice extent (see Atkinson et al. 2004) and given that links have been made between winter sea ice extent in the Southern Ocean and body condition of humpback whales (*Megaptera novaeangliae*) in Western Australia (Braithwaite et al. 2015), the mean September Antarctic sea ice extent (SASIE) was used as the final climatic variable. The month of September was chosen specifically, since it is considered the month where the maximum sea ice extent is found in Antarctica (Nicol et al. 2008). Data for SASIE were obtained from the National Snow & Ice Data Center (NSIDC) (https://nsidc.org/data/seaice_index/).

Ocean colour

Hlista et al. (2009) used satellite-derived sea-surface chlorophyll concentrations as a proxy for the nutritional potential of North Atlantic right whale (*Eubalaena glacialis*) feeding grounds, and successfully explained 50% of the variation in breeding success. Given that chlorophyll *a* is considered the most common measure of the food environment for copepods (Bunker & Hirst 2004) and that studies have found positive relationships between chlorophyll *a* and copepods (Kiørboe & Nielsen 1994, Shreeve et al. 2002) and between chlorophyll *a* and krill (Atkinson et al. 2004, 2008), this study used measures of chlorophyll *a* concentrations in three postulated feeding grounds of SRW (*Figure 2*) as a proxy for SRW prey availability. The strong seasonality in SRW feeding (Best & Schell 1996) indicates that SRWs typically feed during summer. As such, maximum summer chlorophyll *a* concentrations, which typically occur in January (see Constable et al. 2014, Fig. 4) were obtained for the three feeding grounds. Chlorophyll *a* concentration data were obtained from the latest version of the European Space Agency (ESA) Ocean Colour Climate Change Initiative (OC-CCI v3.1) (https://www.oceancolour.org/). The Ocean Colour CCI produces long-term multi-sensor time series of satellite ocean colour data. The OC-CCI chlorophyll *a* product has the units of mg/m^3 and is provided with a horizontal resolution of ~4km/pixel. The January chlorophyll *a* concentration for a random 10% of the available coordinate grid squares were obtained from 1998–2018 for each of the three feeding grounds. The mean chlorophyll *a* concentrations for each of the three 10% samples were then calculated. The map of postulated SRW feeding grounds (*Figure 2*) was created using

QGIS version 2.18.20 (QGIS Development Team, 2009).

Wavelet analyses

Many correlative techniques used to explore time series data make the assumption of stationarity (Cazelles et al. 2008) i.e. statistical properties such as the mean and variance are constant over time. Wavelet analyses, which is able to account for non-stationary data, provide an effective method to investigate the cyclicity of a univariate time series (i.e. wavelet power), as well as potential synchrony (i.e. cross-wavelet power) between two time series (Rosch and Schmidbauer, 2018). Wavelet analyses decomposes a given time series into a continuous range of cycles, to investigate firstly, the presence and power of statistically significant cycles in the time series, and secondly, the potential cyclicity that is common between two time series (i.e. synchrony). As such, wavelet power plots delineate clusters of significant cycles occurring in the time series during a certain time interval, whereas cross-wavelet power plots delineate clusters of significant cycles that are common in both time series at a certain time interval. Wavelet power spectra were calculated for the cow-calf pair count time series and all climate index time series (including chlorophyll *a* data for the three postulated feeding grounds). The cow-calf pair count data were log transformed in order to amplify any cycles found in the time series where low population sizes are present (evident in the 1970s-1980s; *see Figure 1*). In order to prevent the overall trends of any time series from interfering with their cyclicity, all time series were also detrended using local polynomial regression with high levels of smoothing (LOESS smooth span = 30%). Given the sharp drop and increase in the cow-calf pair counts after 2014 (i.e. the "crash") (*Figure 5 A*), the wavelet power spectrum for the cow-calf pair count time series was computed separately for data including and excluding the "crash" (1972-2018 and 1972-2014 respectively). This was done to isolate the signal from the strong fluctuations after 2014 which overwhelms the earlier cycles in the cow-calf pair count time series. Wavelet power spectra were thus computed for the log transformed and detrended cow-calf pair counts, including and excluding the crash; as well as all detrended climate indices (including chlorophyll *a* concentrations for the three postulated feeding grounds).

Additionally, cross-wavelet power spectra were computed for the log transformed and detrended cow-calf pair counts with all climate indices (including chlorophyll *a* data for the three postulated feeding grounds), including and excluding the "crash". Furthermore, information about the synchronisation of the two series is given in the cross-wavelet power plots in the form of arrows, indicating the instantaneous phase difference between the two time series. Arrows pointing right or left at 180° indicate two time series that are moving perfectly in phase (i.e. when *x* increases, *y* increases) or in anti-phase (i.e. when *x* increases, *y* decreases) respectively. Two time series that move in phase or in anti-phase, but with one time series leading/lagging the other, are represented by all other arrow directions, indicating their phase differences. *Figure 3* illustrates two time series moving in phase and completing a single cycle. From this figure, it is clear that *x* is leading *y* by angle *a*. However, if the size of *a* were to increase, one would be able to interpret the figure as the two series are moving in anti-phase, with *y* leading *x*. As such, the interpretations of the cross-wavelet arrow directions are cyclic in nature (leading by *a* is equivalent to lagging by $2\pi - a$). Wavelet and cross-wavelet power spectra were computed in R version 3.5.1

(R Core Team, 2018) using the WaveletComp (version 1.1) package (Rosch and Schmidbauer, 2018).

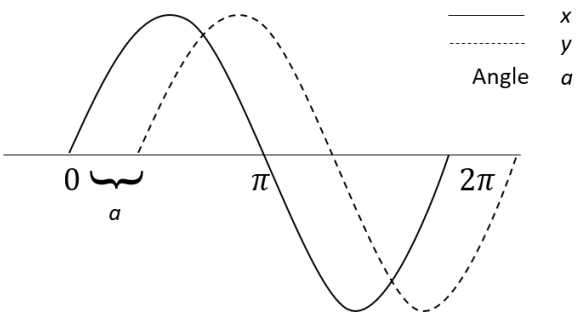

Figure 3 Schematic diagram illustrating two time series moving in phase and each completing one full cycle. Series *x* currently leads series *y* by an order of angle *a*.

ARIMA modelling

(i) Environmental variable lag selection

In order to account for potentially delayed effects between climate indices (and chlorophyll *a* concentrations) and the counts of cow-calf pairs, the various environmental variables were lagged. The quantity of lag to be used for each environmental variable was decided based on the phase difference results of the cross-wavelet power plots. *Figure 4* illustrates a hypothetical scenario of two time series, each completing a cycle with a period of 2π.

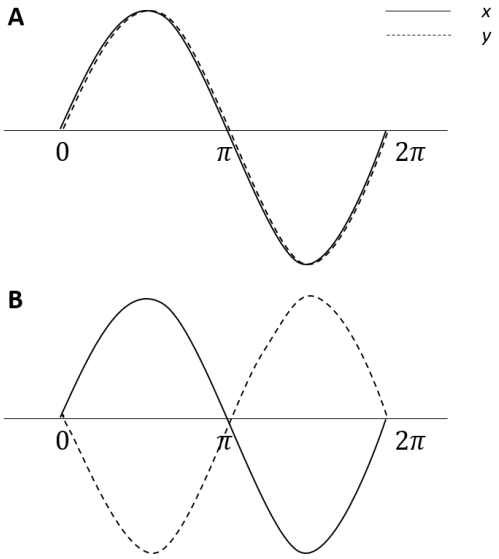

Figure 4 Schematic diagram illustrating two time series (*x* and *y*) each completing a cycle with a period of 2π, while moving: **A)** perfectly in phase, with neither series *x* nor series *y* leading/lagging; and **B)** perfectly in anti-phase, with neither series *x* nor series *y* leading/lagging.

The time series in *Figure 4 A* are moving perfectly in phase, with neither *x* nor *y* leading/lagging. In this scenario, no lags exist between the possible effect of *x* on *y*. Therefore: $y_t = ARIMA_{errors} + x_t$

The time series in *Figure 4 B* are moving perfectly in anti-phase, with neither *x* nor *y* leading/lagging. In order for

the time series in *B* to reach a perfect synchronisation as seen in *A*, *x* needs to be shifted by π. Thus, π represents the maximum amount of lag that can occur between two time series which share a common cycle. Therefore: $y_t = ARIMA_{errors} + x_{t-\pi}$.

However, the cross-wavelet power analyses are unlikely to produce results as seen in this hypothetical example. Thus, in order to account for all possible lags that can occur within one cycle between the various climate indices and the cow-calf pair counts, lags were added to the ARIMA models sequentially, up until the highest possible lag. This can be written as: $y_t = ARIMA_{errors} + x_t + x_{t-\ldots} \ldots + x_{t-\pi}$

In other words, when assessing the maximum amount of lag to generate for the potential association between cow-calf pair counts and an environmental variable, the highest significant cyclic periodicity found between the two time series was taken as 2π. Thus, the maximum amount of lag generated for the association between cow-calf pair counts and the respective environmental variable would be equal to $2\pi/2$.

(ii) ARIMA models

The response variable used in the ARIMA models was the deviation of SRW cow-calf pair counts from the 6.9% annual population growth rate (i.e. growth rate anomalies), which was valid up until at least 2006 (Best et al. 2010). Given that the climate index data for the ONI, AAO and SASIE are up to 26 years longer (ONI: 1972-2018) compared to that of the chlorophyll data (1998-2018), separate ARIMA models were generated for these two sets of data. In addition, cow-calf pair growth rate anomalies including the "crash" (1972-2018) and excluding the "crash" (1972-2014) were analysed separately. Therefore, 4 main groups of ARIMA models were constructed: (1) Growth rate anomalies and the ONI, AAO and SASIE; including the "crash". (2) Growth rate anomalies and chlorophyll *a* concentrations from postulated feeding ground A, B and C; including the "crash". (3) Growth rate anomalies and the ONI, AAO and SASIE; excluding the "crash". (4) Growth rate anomalies and chlorophyll *a* concentrations from postulated feeding ground A, B and C; excluding the "crash". The ARIMA model error structure is in the form of (*p*, *d*, *q*), where *p* refers to the number of autoregressive terms (AR), *d* refers to the differencing order and *q* refers to the number of moving average terms (MA). Autocorrelation plots (ACF) and partial autocorrelation plots (PACF) of the growth rate anomaly time series were used to determine the order of *p* and *q*. The PACF is used to determine the AR order which is *p*, while the ACF determines the MA order which is *q*. The Augmented Dickey-Fuller (ADF) test was then used to determine whether the residuals of the chosen model were stationary. If the stationarity test failed, a differencing order of *d=1* was applied to the growth rate anomalies, and the ACF and PACF were reanalysed to determine the new order of *p* and *q*. This process was repeated until the correct starting ARIMA model was obtained for each of the four model classes. Predictor variables with their respective lags were incorporated into the original model in two different ways: firstly, by adding one variable at a time and adding the lags sequentially; and secondly, with all variables at all lags included from the start, followed by removing one variable at a time. In order to include predictor variables at their maximum lags and, given that the lengths of the climate index data vary, the length of data used in each of the model classes was standardized (i.e. the maximum length of data without any missing values was included). This was done to allow accurate comparisons between models using the same amount of data. Model validation (ACF and PACF of growth rate anomalies, ACF of model residuals and ADF test results) were obtained

for each model. Finally, in order to assess potential improvement in model performance after adding environmental predictor variables, AIC scores and adjusted R^2 values were compared between models within each model class. Significant model performance improvement was calculated by assessing whether the delta AIC was significantly different, based on the one-tail chi-square test (for upper tail) with the dimension *n* (*n* refers to the difference in parameter numbers between the two models). For example, if a model with no predictor variables is compared to a model with 4 predictor variables, then *n* = 4 and, based on the chi-square test, a delta AIC > 9.48 is required for the difference to be significantly different (at the 0.05 significance level). ARIMA models were computed using R version 3.5.1 (R Core Team, 2018) using the *tseries* (version 0.10.46) package (Trapletti and Hornik, 2018) and the *forecast* (version 8.5) package (Hyndman et al. 2019).

Results

Southern right whale counts

The counts of unaccompanied adults ranged between 9 and 433 (in the years 2016 and 2008 respectively) while the cow-calf pair counts ranged between 21 and 537 (in the years 1973 and 2018 respectively) (*Figure 1*). The clear increasing trends in the count data for both demographic groups of whales deviate for the first time after 2008, with merely 9 unaccompanied adults counted in 2016. This trend of unusually low numbers of unaccompanied adults continues till 2018. In contrast however, counts of cow-calf pairs deviated drastically from the trend after 2014, with 55 cow-calf pairs counted in 2016. Counts of cow-calf pairs increased the following year, with a record-high number of cow-calf pairs of 537 in 2018.

Wavelet analyses

(i) Wavelet power

The counts of cow-calf pairs, excluding the “crash”, fluctuated with a cyclic periodicity of 3-4 years (*Figure 5 C*). This periodicity was not constant over time, with the strongest cycles occurring between 1974 and 1987. The 3-4-year periodicity was insignificant for a large portion of the remainder of the time series, apart from small clusters of significance between 1997-2001 and 2008-2009. In contrast, the counts of cow-calf pairs, including the “crash”, fluctuate with much more variance starting from 2009 (*Figure 5 B*). The first cycle seen in the large significant cluster (2009-2016), begins in 2009 and fluctuates at a 5-6-year periodicity. The peak in the cycles (i.e. the strongest wavelet power) has a cyclic periodicity of 3-5 years, starting in 2015. The 3-7-year range of cyclic periodicity found in this cluster likely overrides the weaker 3-year cycles which can be seen in *Figure 5 C*. Despite the drastic fluctuations in cycles starting in 2009, a small cluster of significance indicating a 3-4-year cyclic periodicity is found between 1977-1980 (*Figure 5 B*).

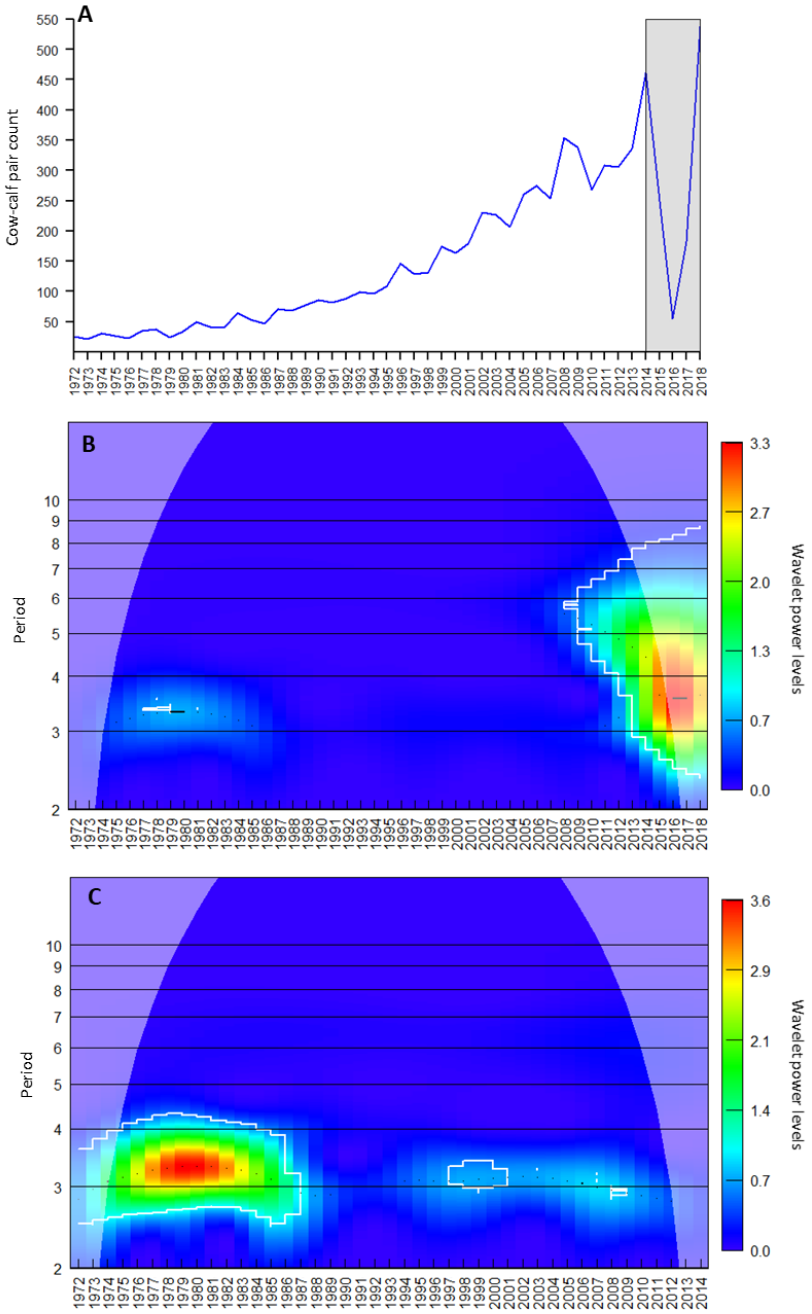

Figure 5 A) Time series of southern right whale cow-calf pair counts (1972 – 2018); shaded area (2014 – 2018) delineates the clear "crash" in the time series. **B)** Wavelet power spectrum of the log transformed southern right whale cow-calf pair count time series, including the "crash" (1972 – 2018). **C)** Wavelet power spectrum of the log transformed southern right whale cow-calf pair count time series, excluding the "crash" (1972 – 2014). Data were first log transformed to amplify the cyclical signals of the small population size found in the early years of the time series. Both time series were detrended using Local polynomial regression (LOESS; 30% smoothing span) to account for any trends in the time series. The null hypothesis of "no periodicity" in these plots was tested with simulation algorithms. White contour lines delineate areas of significant periodicity ($p<0.1$). The shaded area indicates the cone of influence, which delimits the region not influenced by edge effects.

The Oceanic Nino Index (ONI) appears to fluctuate predominantly with a cyclic periodicity of 4-6 years, especially between 1975 and 1994 (*Figure A1 A*). However, cycles with a period of around 3 years can be seen between 1995 and 2000, and from 2009 onwards. The Antarctic Oscillation (AAO) has two distinct clusters of significant cycles (*Figure A1 B*): a cyclic periodicity of 4-6 years between 1990 and 2000, followed by a more frequent cyclicity of 2-3 years between 2000 and 2013. The September Antarctic sea ice extent (SASIE) has a weak but significant cyclic periodicity around 7 years from 1999 onwards (*Figure A1 C*). There are also two cycles with a shorter period between 1982 and 1987, and 2008 onwards, at 2-3 years and 4-5 years respectively. The chlorophyll *a* concentrations for postulated feeding grounds A, B and C show similar cyclic periodicity (*Figure A1 D;E;F*), with all significant clusters ranging between a periodicity of 2-3 years. The cycles however are not constant throughout time; feeding ground A has significant cyclic periodicity between 2000 and 2013; feeding ground B has significant cyclic periodicity between 2000 and 2009, and from 2015 onwards; and feeding ground C has significant cyclic periodicity between 2002 and 2013.

(ii) Cross-wavelet power

Synchrony was found between the cycles of cow-calf pair counts (excluding and including the "crash") and all climate indices (including chlorophyll *a* concentrations).

ONI: The ONI and cow-calf pair count cross-wavelet results indicate significant synchrony, with the cycles of the two time series moving mostly in anti-phase (*Figure 6 B,C*). Clusters of significant cycle synchrony between the ONI and cow-calf pair data excluding the "crash" are found predominantly with a periodicity of 3-4 years, between 1975 and 1997, 1995 and 2000, and 2008 and 2011 (*Figure 6 C*). When including the "crash", only one cluster of significant cycle synchrony is found, with a periodicity of 3-6 years, from 2010 onwards (*Figure 6 B*).

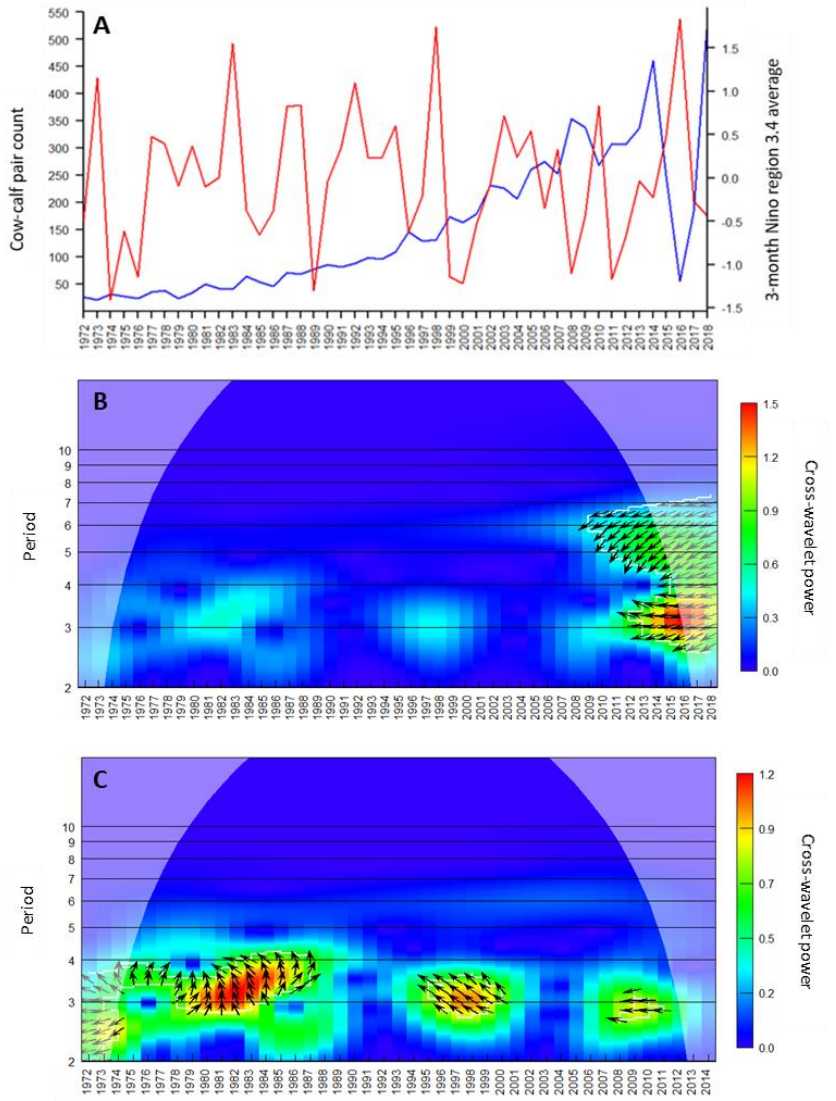

Figure 6 The cycle synchrony between log and detrended cow-calf pair counts, including and excluding the "crash" and the Oceanic Niño Index. **A)** Blue line: time series of southern right whale cow-calf pair counts, including the "crash" (1972 – 2018); red line: time series of the Oceanic Nino Index (1972 – 2018). **B)** Cross-wavelet power plot illustrating the synchrony in the cycles of southern right whale cow-calf pair counts including the "crash" (1972 – 2018) and the Oceanic Niño Index. **C)** Cross-wavelet power plot illustrating the synchrony in the cycles of southern right whale cow-calf pair counts excluding the "crash" (1972 – 2014) and the Oceanic Niño Index. Cross-wavelet power plots identify period bands and time intervals within which the cycles of the two time series are synchronised. The shaded area indicates the cone of influence, which delimits the region not influenced by edge effects. White contour lines border areas of significance. P-values associated with the values within the region delineated by the white contour lines are less than 5%.

AAO: The cycles of the AAO are synchronized with that of the cow-calf pair data excluding the "crash" from 1993 to 2011 (*Figure 7* C). The synchrony is found for mostly a 3-year period, with the cycles moving in phase. However, when including the "crash", cycle synchronicity is found from 2012 onwards, with the cycles moving in anti-phase (*Figure 7 B*).

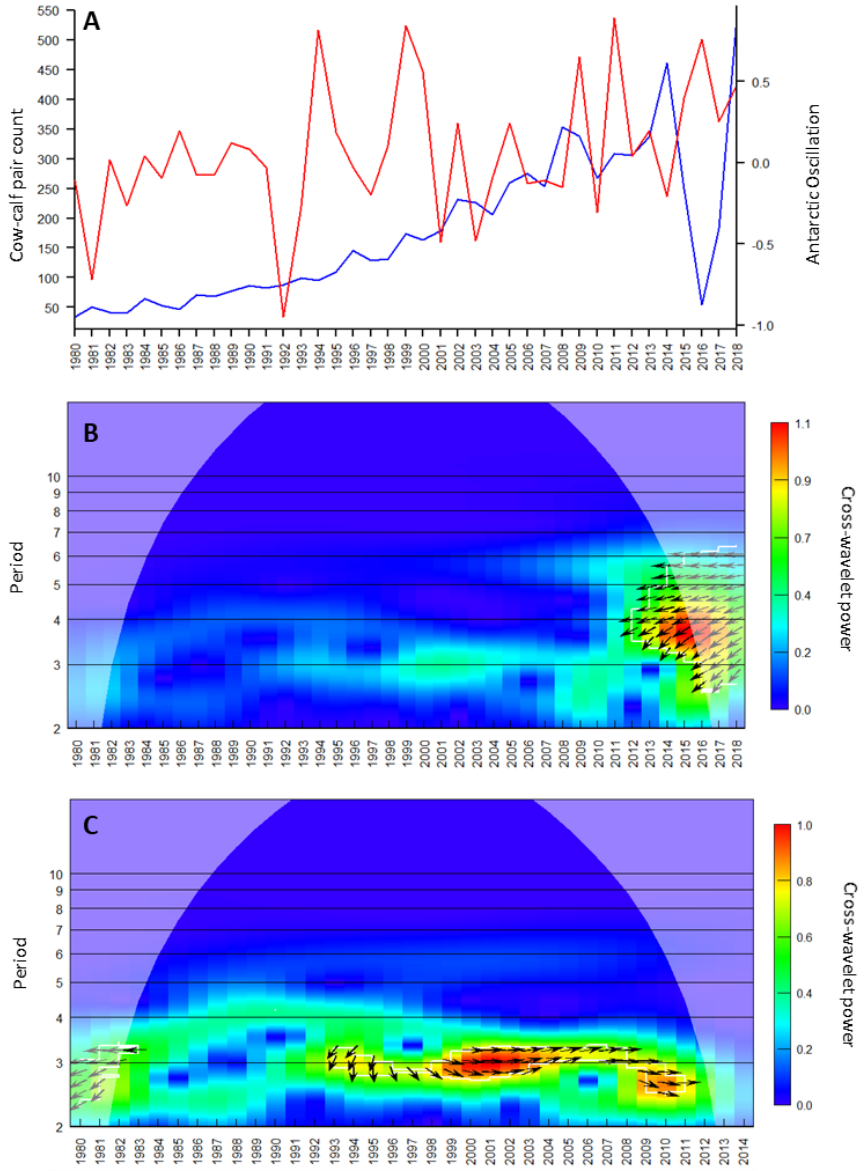

Figure 7 The association between log and detrended cow-calf pair counts, including and excluding the "crash" and the Antarctic Oscillation. **A)** Blue line: time series of southern right whale cow-calf pair counts, including the "crash" (1980 – 2018); red line: time series of the Antarctic Oscillation (1980 – 2018). **B)** Cross-wavelet power plot illustrating the synchrony in the cycles of southern right whale cow-calf pair counts including the "crash" (1980 – 2018) and the Antarctic Oscillation. **C)** Cross-wavelet power plot illustrating the synchrony in the cycles of southern right whale cow-calf pair counts excluding the "crash" (1980 – 2014) and the Antarctic Oscillation. Cross-wavelet power plots identify period bands and time intervals within which the cycles of the two time series are synchronised. The shaded area indicates the cone of influence, which delimits the region not influenced by edge effects. White contour lines border areas of significance. P-values associated with the values within the region delineated by the white contour lines are less than 5%.

SASIE: The SASIE and cow-calf pair counts excluding the "crash" have two distinct clusters of synchronicity (*Figure A2 C*). The first cluster, between 1981 and 1989, has cycles at a 4-year periodicity moving in phase, while at a 2-3-year periodicity, the cycles move in anti-phase. The second cluster, between 1999 and 2011, has one predominant cyclic periodicity of 3 years, with the cycles moving in anti-phase. However, when including the "crash", a single cluster of synchronicity is found, with cycles of a 3-7-year period moving in phase (*Figure A2 B*).

Chlorophyll *a*: Cross-wavelet power plots for the chlorophyll *a* concentrations and cow-calf pair counts excluding the "crash" revealed little synchrony in their cycles. Significant synchrony for chlorophyll *a* in postulated feeding ground A is found at a 2-4-year periodicity from 2000-2001, with the cycles moving in phase (*Figure A3 C*). Significant synchrony for chlorophyll *a* in postulated feeding ground B is found at 2-3-year periodicity from 2000-2001, with the cycles moving in anti-phase (*Figure A4 C*). Postulated feeding ground C has only a single year (2000) of significant cycle synchrony, with the cycles moving in phase at a 2-3-year periodicity (*Figure A5 C*). In contrast, cycle synchronicity for longer time intervals can be seen in the cross-wavelet power plots for the chlorophyll *a* concentrations and cow-calf pair counts including the "crash". Chlorophyll *a* concentration cycles from postulated feeding ground A is in synchrony with cow-calf pair counts including the "crash" between 2008 and 2016, with a cyclic periodicity between 2 and 4 years (*Figure A3 B*). Phase difference arrows indicate that at a 3-4-year periodicity, cycles move in anti-phase, while at a 2-3-year periodicity, cycles move in phase. Postulated feeding ground B has a short time interval of cycle synchronicity with cow-calf pair counts including the "crash", with significant anti-phase moving cycles at a 2-3-year period found from 2014 onwards (*Figure A4 B*). Postulated feeding ground C has two clusters of significant cycle synchrony with cow-calf pair counts including the "crash" (*Figure A5 B*): the first, from 2009-2011, has a cyclic periodicity of 3 years and phase difference arrows indicate that the synchrony is at the edge of both in phase and anti-phase movement; the second, from 2014-2016, has a cyclic periodicity of 2-3-years and phase difference arrows indicate mostly in phase movement.

ARIMA models

For the first class of ARIMA models (growth rate anomalies and the ONI, AAO and SASIE; including the "crash"), an original ARIMA model order of (4,3,6) was computed (*Table 1 Model 1*). The ADF test of model residuals indicated stationarity ($p < 0.05$). The model explained high amounts of variation in growth rate anomalies (AIC = 12.69, adjusted $R^2 = 0.6961$). Lagged climatic variables were added sequentially to this original model; ONI (up to 3 years lag), AAO (up to 3 years lag) and SASIE (up to 4 years lag) (*Table 1 Model 2-14*). Stationarity issues for data including the "crash" were expected due to the drastic drop and subsequent rise in the count data. These issues are realized through the ADF tests of model residuals indicating stationarity for model 5,6,7,9 and 10 ($p < 0.05$) while model 2,3,4,8,11,12,13 and 14 did not pass the test ($p > 0.05$). A number of models performed significantly better than the original model, however. The best performing model for each climate variable included model 2 for ONI and model 8 for AAO (see *Table 1*). The second method of incorporating lags into the original ARIMA model yielded models which all outperformed the original model, however only model 27 yielded a significant delta AIC (see *Table 2*). As expected, ADF tests of model residuals indicated non-stationarity for models 25-28 ($p > 0.05$).

Table 1 ARIMA model results for the first lag incorporation method. Models 1-14: first class of ARIMA models: growth rate anomalies and the ONI, AAO and SASIE; including the "crash". Models 15-24: second class of ARIMA models: growth rate anomalies and chlorophyll *a* concentrations from postulated feeding ground A, B and C; including the "crash". Significant model performance improvement compared to the original model (excluding predictors) is indicated via * (0.1 significance level) and ** (0.05 significance level).

Model number	Length of Data	Model Order / Predictors	Log Likelihood	AIC	Adjusted R^2
1	1983-2018	(4, 3, 6)	4.66	12.69	0.6961
2	1983-2018	(4, 3, 6) / ONI*(t)*	11.08	1.84 **	0.8006
3	1983-2018	(4, 3, 6) / ONI*(t)* + ONI*(t-1)*	11.09	3.82 **	0.7992
4	1983-2018	(4, 3, 6) / ONI*(t)* + ONI*(t-1)* + ONI*(t-2)*	12.37	3.26 **	0.8507
5	1983-2018	(4, 3, 6) / ONI*(t)* + ONI*(t-1)* + ONI*(t-2)* + *ONI(t-3)*	4.68	20.63	0.7721
6	1983-2018	(4, 3, 6) / AAO*(t)*	2.96	18.09	0.7594
7	1983-2018	(4, 3, 6) / AAO*(t)* + AAO*(t-1)*	4.37	17.26	0.7816
8	1983-2018	(4, 3, 6) / AAO*(t)* + AAO*(t-1)* + AAO*(t-2)*	11.86	4.28 **	0.8447
9	1983-2018	(4, 3, 6) / AAO*(t)* + AAO*(t-1)* + AAO*(t-2)* + *AAO(t-3)*	9.22	11.56	0.7619
10	1983-2018	(4, 3, 6) / SASIE*(t)*	5.26	13.49	0.7044
11	1983-2018	(4, 3, 6) / SASIE*(t)* + SASIE*(t-1)*	0.42	25.16	0.7174
12	1983-2018	(4, 3, 6) / SASIE*(t)* + SASIE*(t-1)* + SASIE*(t-2)*	5.4	17.2	0.8066
13	1983-2018	(4, 3, 6) / SASIE*(t)* + SASIE*(t-1)* + SASIE*(t-2)* + *SASIE(t-3)*	5.42	19.16	0.8010
14	1983-2018	(4, 3, 6) / SASIE*(t)* + SASIE*(t-1)* + SASIE*(t-2)* + *SASIE(t-3)* + *SASIE(t-4)*	11.12	9.76	0.8029
15	2000-2018	(1, 0, 1)	-1.33	10.67	0.4815
16	2000-2018	(1, 0, 1) / Ground A*(t)*	-0.58	11.17	0.5214
17	2000-2018	(1, 0, 1) / Ground A*(t)* + Ground A*(t-1)*	0.15	11.71	0.5580
18	2000-2018	(1, 0, 1) / Ground A*(t)* + Ground A*(t-1)* + Ground A*(t-2)*	0.83	12.35	0.5863
19	2000-2018	(1, 0, 1) / Ground B*(t)*	-0.46	10.91	0.5807
20	2000-2018	(1, 0, 1) / Ground B*(t)* + Ground B*(t-1)*	-0.41	12.82	0.5812
21	2000-2018	(1, 0, 1) / Ground B*(t)* + Ground B*(t-1)* + Ground B*(t-2)*	1.53	10.95	0.6673
22	2000-2018	(1, 0, 1) / Ground C*(t)*	-0.86	11.72	0.5068
23	2000-2018	(1, 0, 1) / Ground C*(t)* + Ground C*(t-1)*	3.53	4.94 *	0.7275
24	2000-2018	(1, 0, 1) / Ground C*(t)* + Ground C*(t-1)* + *Ground C(t-2)*	3.8	6.39	0.7084

Table 2 ARIMA model results for the second lag incorporation method. Models 1-28: first class of ARIMA models: growth rate anomalies and the ONI, AAO and SASIE; including the "crash". Significant model performance improvement compared to the original model (excluding predictors) is indicated via * (0.1 significance level) and ** (0.05 significance level).

Model number	Length of Data	Model Order / Predictors	Log Likelihood	AIC	Adjusted R^2
1	1983-2018	(4, 3, 6)	4.66	12.69	0.6961
25	1983-2018	(4, 3, 6) / ONI*(t)* + ONI*(t-1)* + ONI*(t-2)* + *ONI(t-3)* + AAO*(t)* + AAO*(t-1)* + AAO*(t-2)* + AAO*(t-3)* + SASIE*(t)* + SASIE*(t-1)* + SASIE*(t-2)* + SASIE*(t-3)* + SASIE*(t-4)*	27.34	-6.69	0.9309
26	1983-2018	(4, 3, 6) / ONI*(t)* + ONI*(t-1)* + ONI*(t-2)* + *ONI(t-3)* + AAO*(t)* + AAO*(t-1)* + AAO*(t-2)* + AAO*(t-3)*	13.76	10.47	0.8847
27	1983-2018	(4, 3, 6) / ONI*(t)* + ONI*(t-1)* + ONI*(t-2)* + ONI(t-3) + SASIE*(t)* + SASIE*(t-1)* + SASIE*(t-2)* + SASIE*(t-3)* + SASIE*(t-4)*	24.3	-8.59 **	0.9258
28	1983-2018	(4, 3, 6) / AAO*(t)* + AAO*(t-1)* + AAO*(t-2)* + AAO*(t-3)* + SASIE*(t)* + SASIE*(t-1)* + SASIE*(t-2)* + SASIE*(t-3)* + SASIE*(t-4)*	19.23	1.55	0.8982

For the second class of ARIMA models (growth rate anomalies and chlorophyll *a* concentrations from postulated feeding ground A, B and C; including the "crash"), an original ARIMA model order of (1,0,1) was computed (*Table 1 Model 15*). The ADF test of model residuals indicated non-stationarity ($p > 0.05$), regardless of the differencing order applied to the model. As such, results originating from this model should be interpreted with caution (*Table 1 Model 15-24*). The model explained relatively low amounts of variation in growth rate anomalies (AIC = 10.67, adjusted R^2 = 0.4815). Lagged chlorophyll variables, added sequentially to this original model, were chlorophyll *a* from postulated feeding ground A, B and C (each up to 2 years lag) (*Table 1 Model 16-24*). Two models performed better than the original model (*Table 1 Model 23;24*), however only the model including chlorophyll *a* from postulated feeding ground C (lagged by 1 year) yielded a significant delta AIC (*Table 1 Model 23*). Due to the lack of long-term data, the second method of lag incorporation was not computed for this second class of ARIMA models.

For the third class of ARIMA models (growth rate anomalies and the ONI, AAO and SASIE; excluding the "crash"), an original ARIMA model order of (3,2,6) was computed (*Table A1 Model 1*). The ADF test of model residuals indicated stationarity ($p < 0.05$). The model explained high amounts of variation in growth rate anomalies (AIC = -62.76, adjusted R^2 = 0.7779). Lagged climatic variables, added sequentially to this original model, were the ONI (up to 2 years lag), the AAO (up to 2 years lag) and the SASIE (up to 2 years lag) (*Table A1 Model 2-10*). ADF tests of model residuals indicated stationarity for all 9 models. The only models which performed better than the original model were models including the AAO (*Table A1 Model 5;6*). However, neither of these models yielded significant delta AICs. The second method of incorporating lags into the original ARIMA model was unable to improve the model performance (*Table A2*). ADF tests of model residuals indicated stationarity for model 20 and 22 ($p < 0.05$) while model 21 and 23 did not pass the test ($p > 0.05$).

For the fourth class of ARIMA models (growth rate anomalies and chlorophyll *a* concentrations from postulated feeding ground A, B and C; excluding the "crash"), an original ARIMA model order of (4,0,0) was computed (*Table A1 Model 11*). The ADF test of model residuals indicated non-stationarity ($p > 0.05$), regardless of the differencing order applied to the model. As such, results originating from this model should be interpreted with caution (*Table A1 Model 11-19*). The model explained high amounts of variation in growth rate anomalies (AIC = -23.31, adjusted R^2 = 0.7005). Lagged chlorophyll variables, added sequentially to this original model, were chlorophyll *a* from postulated feeding ground A, B and C (up to 2 years, 2 years and 1 year lag respectively) (*Table A1 Model 12-19*). Two models performed better than the original model (*Table A1 Model 14;17*), however neither of these models yielded significant delta AICs. Due to the lack of long-term data, the second method of lag incorporation was not computed for the fourth class of ARIMA models.

Model validation for all ARIMA models (ACF and PACF of growth rate anomalies, ACF of model residuals) were obtained but are not included in this report.

Discussion

Three-year calving cohort

SRW females have a calving interval of approximately three years and, as such, 3 three-year "cohorts" have been observed in the count data, where every three years one of the 3 cohorts will be calving. Since the number of females in each cohort varies, so too will the number of calves born each year co-vary, thus maintaining an observed 3-year periodicity. Through visual inspection of the count data, a "bumper-cohort" was noted up to 2010, where every 3 years a larger cohort of females gave birth. However, this "bumper-cohort" signature is dissipated after 2010, most likely due to an increasing occurrence of 4- and 5-year calving intervals (as opposed to the normal 3-year intervals), which have become the norm since 2015 (Vermeulen et al. 2018). Interestingly, the 3-4-year cyclic periodicity found in the cow-calf pair counts excluding the "crash" provides the first statistical evidence for this "bumper-cohort" in SRW females, with the large "bumper-cohort" completing a breeding cycle every 3-4 years. This 3-4-year cyclical signal, which although not significant throughout, is evident for most of the time series (apart from a time interval between 1987 and 1997), with the signal dissipating after 2010. When including the "crash" in the analyses, a wide range of cyclic periodicities can be seen from 2009 onwards, with the strongest cycles occurring with a period of 3-5-years from 2015 onwards. The first appearance of these strong 3-5-year cycles occur within the 'cone of influence' and thus can be interpreted with some confidence. The cycles suggest a shift in calving intervals from a 3-year cycle a to a 4- and 5-year cycle as found by Vermeulen et al. (2018). Thus, the wavelet analyses for the cow-calf pair counts provide evidence for the presence of the large "bumper-cohort", when excluding the "crash". Secondly, evidence is provided for the dissipation of this "bumper-cohort" signal from 2009 onwards, due to an increasing length in calving intervals of SRW females. It must be noted that the shift found in calving interval length (Vermeulen et al. 2018), together with the drastic fluctuations in the cycles of cow-calf pair counts found in this study, begins around 2009/2010 – the same years where the counts of unaccompanied SRW adults dropped sharply. As such, there appears to have been synchrony in the timing of the increasing calving intervals of SRW females and the absence of unaccompanied SRW adults along South Africa's southern coast. This synchrony is unlikely to be coincidental and will be addressed at a later stage in this discussion.

Influence of environmental variables on cow-calf pair counts

Results presented in this document reveal that the Antarctic Oscillation (AAO) may play a role in the inter-annual fluctuations of SRW cow-calf pair counts. As mentioned previously, the AAO is the leading mode of atmospheric variability south of 20^{o}S (Pohl et al. 2010, Salinger et al. 2016). Winds associated with the AAO alter the circulation patterns of the Southern Ocean which can ultimately influence the abundance of phytoplankton (Lovenduski & Gruber, 2005). A large variety of zooplankton (the most common of which are copepods and krill) are in turn sustained by phytoplankton (Duxbury, Duxbury and Sverdrup K.A, 1999). Cross-wavelet power results for cow-calf pair count cycles excluding the "crash" revealed significant synchrony with the cycles of the AAO from 1993 to 2011. The synchronicity spans most of the time series with a cyclic periodicity of 3-years, with what appears to be perfect in phase movement. These results suggest a positive association between the AAO and cow-calf pair counts without any lags between the signals. Despite no significant model performance

improvement being found through the inclusion of any climatic predictor variables when excluding the "crash", the ARIMA model including the AAO_t as the only climatic predictor performed the best out of all potential models. Results further suggest that chlorophyll *a* concentrations in postulated feeding ground A and B may also play a role in the inter-annual fluctuations of SRW cow-calf pair counts up to a 2 year lag. Similar findings have been seen elsewhere. For example, a study conducted on North Atlantic right whales revealed significant correlations between the number of right whale calves born and chlorophyll concentrations averaged over the prior 2 years (Hlista et al. 2009). Similarly, Greene et al. (2003) found that the abundance of a copepod species (*Calanus finmarchicus*) was significantly correlated at 0- and 2-year lags to the calving rates of North Atlantic right whales. The mechanistic links between chlorophyll and right whale feeding success however, are inherently complex and mediated by various environmental and biological processes, such as potentially complex life histories of various prey species (Hlista et al. 2009).

As mentioned previously, the El Niño–Southern Oscillation (ENSO) has been found to show strong links with sea ice extent in Antarctica (Loeb et al. 2009, Loeb & Santora 2015) and as a result, impacts krill densities (Loeb et al. 1997, Fraser & Hofmann 2003, Atkinson et al. 2004, Flores et al. 2012, Trathan et al. 2012). Thus, there is cause for concern for the potential role of El Niño events in driving some of the recent trends in South Africa's population of SRW. The impact of El Niño events on SRWs is thought to be mediated through the effect of elevated SSTs (typical of El Niño conditions) on the variation in SRW food availability (Leaper et al. 2006, Seyboth et al. 2016). Loeb & Santora (2015) analysed 18 years of krill data near the North Antarctic Peninsula and found that the post-larval and larval abundance of four different krill species increased during a time period associated with a shift from El Niño to La Niña (or "Niño-neutral") dominated conditions. Interestingly, wavelet power analyses revealed an increased frequency in the cycles of the ONI since 2009. This increased frequency can be seen with most of the ONI time series initially being dominated by a 4-6-year cycle up until 2000, with a 3-year cycle seen between 1995 and 1999, and from 2009 onwards. This result concurs with models which have suggested that El Niño-like conditions are likely to increase in frequency over the coming decades (Holmgren et al. 2001). Cross-wavelet power analyses revealed significant synchrony between the ONI and cow-calf pair count cycles. When excluding the "crash", three clusters of significance were found, with the cycles in all three cases moving mostly in anti-phase. The cross-wavelet power strength of these clusters indicates high power around the years of 1982 and 1998, with weaker power in the third cluster around 2010. All three of these clusters occur during times of El Niño conditions. 1982/1983 and 1997/1998 were both periods of very strong El Niño's, while the El Niño of 2010/2011 was moderately strong. The anti-phase movement of the cow-calf pair count and ONI cycles suggest a negative association between El Niño conditions and cow-calf pair counts. However, as no model improvement was found when including lagged ONI values in the ARIMA model excluding the "crash", the ONI does not appear to have a prominent role in driving inter-annual fluctuations in cow-calf pair counts when excluding the "crash".

When including the "crash" in the data, however, a large cluster of significant anti-phase cycle synchrony can be found between the ONI and cow-calf pair counts from 2011 onwards, with the highest cross-wavelet power

occurring around 2015. This time interval corresponds to the extreme 2015/2016 El Niño event, which has been referred to as a "super El Niño" (Chen et al. 2017). Furthermore, when including ONI values lagged by up to 2 years in the ARIMA model including the "crash", significant model performance improvement can be seen. Thus, the ONI, and hence El Niño events, with a lag of up to 2 years may have played a role in the "crash" of cow-calf pair counts along the South African coast. El Niño events have explained reductions in reproductive success of predators in the Antarctic before. For example, the frequent El Niño events between 1987 and 1998 resulted in reductions in Antarctic fur seal pup production for more than 20 years (Forcada et al. 2005). While the time scale at which these El Niño signals are propagated poleward and the lag times that exist in the system require further research (Turner 2004), associations between the ONI and cow-calf pair counts at various lags can be expected. This is due to the time delay between elevated SSTs occurring in the Pacific and the El Niño signal being propagated into the Southern Ocean, in addition to the time it would take for altered food availability to reflect in SRW cow-calf pair counts along a stretch of South African coastline. However, the intense El Niño event of 1997-1998 was found to have strong, direct effects on the Atlantic region of the Southern Ocean with a lag time of less than 6 months (Murphy et al. 2007). This finding illustrates that it is in fact possible for El Niño events to impact food availability in the Southern Ocean rapidly after occurring.

Association and causation

Providing a potential climate-related explanation to the recent "crash" in cow-calf pair counts is expected to be fairly intuitive when assessing the data for the climate index which is considered to be 'responsible'. For example, if one were to find fluctuations in the cycles of a climate index which reaches far outside of its historic ranges around the time of the "crash" in cow-calf pair counts, then one might be able to suggest a potential causative relationship involving that climate index. In this study, while the inclusion of some climate indices were able to improve ARIMA model performance, and thus are likely to be playing some role, there are still no clear explanations or single climatic drivers which could potentially explain the drastic "crash" in cow-calf pair counts along the South African coast. This is illustrated by the ONI for example, whose inclusion in the ARIMA model without any lag times yields the best performing model. And while its inclusion appears to improve model performance substantially, the result may be largely driven by the synchrony in the timing of the "super El-Niño" of 2015/2016 and the extremely low counts of cow-calf pairs in those same years. However, El-Niños of similar strength have been recorded before, such as the El-Niños of 1982/1983 and 1997/1998, and in both cases, extreme crashes in cow-calf pair counts were not observed. This might well be explained by the already relatively low population sizes of SRW occurring during those years (as SRW were still in the initial stages of recovering from historic whaling). Nonetheless, the correlative nature of the time series approaches used in this study raises some uncertainties regarding the roles that are played by climatic and biological variables in the drastic "crash" in SRW cow-calf pair counts along the coast of South Africa. But, despite the lack of causative response models, which are arguably only acquired through controlled experiments, investigating the potential associations between climate (and biological) variability and the drastic "crash" in cow-calf pair counts is the first step in elucidating mechanistic explanations.

Influence of combinations of environmental variables on cow-calf pair counts

ARIMA model results for data including the "crash", which investigate the potential role of combinations of climate indices, reveal the best performing model includes the ONI lagged up to 2 years and SASIE lagged up to 4 years. The combined effect of a number of climatic drivers leads towards a potential threshold explanation for the "crash", where a combination of drivers such as frequent El Niño's and the melting of sea ice in parts of the Antarctic, may have led to poor feeding conditions in SRW feeding grounds in the Southern Ocean. Given the 3-year reproductive cycle of SRWs, it is likely that feeding conditions over several years are integrated when determining if and when a female SRW might reproduce (Greene et al. 2003). Thus, it is probable that the required body condition for successful reproduction is achieved through cumulative energy storage over several consecutive years of abundant food (Seyboth et al. 2016). As such, poor body condition, caused by several years of poor food availability, may have forced females to take extra years of recovery, allowing more time for them to build up sufficient fat reserves for their following pregnancies. This hypothesis is supported by the increasing occurrence of 4- and 5-year calving intervals of SRW females (Vermeulen et al. 2018). As such, females may have been able to withstand successive years of poor feeding conditions, while continuing to breed, by increasing the time taken between each successive calving event, allowing them more time to feed. It is also likely that females have made extensive use of their fat reserves to sustain themselves during these periods of poor feeding conditions. Evidence of this is provided with recent photo-ID data revealing unusually thin females with calves in the 2 years preceding the "crash" of unaccompanied adults and cow-calf pairs (2008 and 2014 respectively; see document SC/68A/SH/xx).

The hypothesis of poor feeding conditions and resilient breeding females (up till a point) is given further support when also taking the drop in the counts of unaccompanied whales into consideration. To do this, one must first understand the various hypotheses as to why SRW migrate to coastlines in the first place (e.g. Norris 1967, Brodie 1975, Evans 1987, Corkeron & Connor 1999). Most of these hypotheses include an increased chance of survival of offspring either due to a reduced predation pressure (Corkeron & Connor 1999), increased SST which increase calf survival (Norris 1967) or energetic benefits for the mother, likely improving maternal investment (Brodie 1975). And so, it is possible that unaccompanied SRW adults are likely less obliged to make the energetically costly migration to the winter breeding grounds, and as such, if experiencing nutritional stress, might not need to migrate all the way to the winter breeding grounds. In stark contrast, female SRW which are pregnant will need to make the migration to the calm, sheltered bays on South Africa's coast to allow their new-born calves the best chance of survival (Elwen & Best, 2004). Thus, due to the synchronous timing between the sharp reduction of SRW unaccompanied adult counts and the increasing calving intervals seen in SRW females, it is possible that the unaccompanied SRW adults had provided us with an early warning to changes occurring in SRW feeding grounds in the Southern Ocean, as well as the extreme nutritional stress that SRW females would soon experience.

Conclusion

The potential linkages between climate variability, physical oceanography, plankton productivity and ultimately

the prevalence of SRWs in the South African breeding ground are complex. The use of yearly mean climate indices (ONI, AAO) and single month averages (SASIE, chlorophyll *a* concentrations) represent a simplified attempt at quantifying the linkages mentioned above. As such, this study should serve as a potential starting point when investigating climate and biological links for South Africa's SRWs, allowing for more robust modelling, and using more detailed and complete data sets, to provide an undoubtedly more accurate understanding of the intricate climatic processes at play in the Southern Ocean, and their eventual impact on SRW.

Main findings

- Wavelet analysis provides evidence for the presence of a large "bumper-cohort" with a 3-4-year cyclicity, evident for most of the cow-calf pair count data.
- This 3-4-year cyclicity dissipates from 2009 onwards, with strong cycles occurring with a period of 3-5-years from 2015 onwards. This is due to an increasing length in calving intervals of SRW females.
- ARIMA time series analyses on data excluding the "crash" in cow-calf pair counts (i.e. excluding 2015-2018) reveal no significant model performance improvement when including environmental variables.
- ARIMA time series analyses on data including the "crash" in cow-calf pair counts (i.e. including 2015-2018) reveal significant model performance improvement through the inclusion of the Oceanic Niño Index, the Antarctic Oscillation and chlorophyll *a* concentration data from one of the three postulated SRW feeding grounds.
- Ultimately, we suggest that the combined effect of several climatic drivers may have led to poor feeding conditions in SRW feeding grounds in the Southern Ocean, which is likely to have played a major role in the recent reversal in the increasing trend of abundance in SRW cow-calf pair counts along the coast of South Africa.

Appendix A

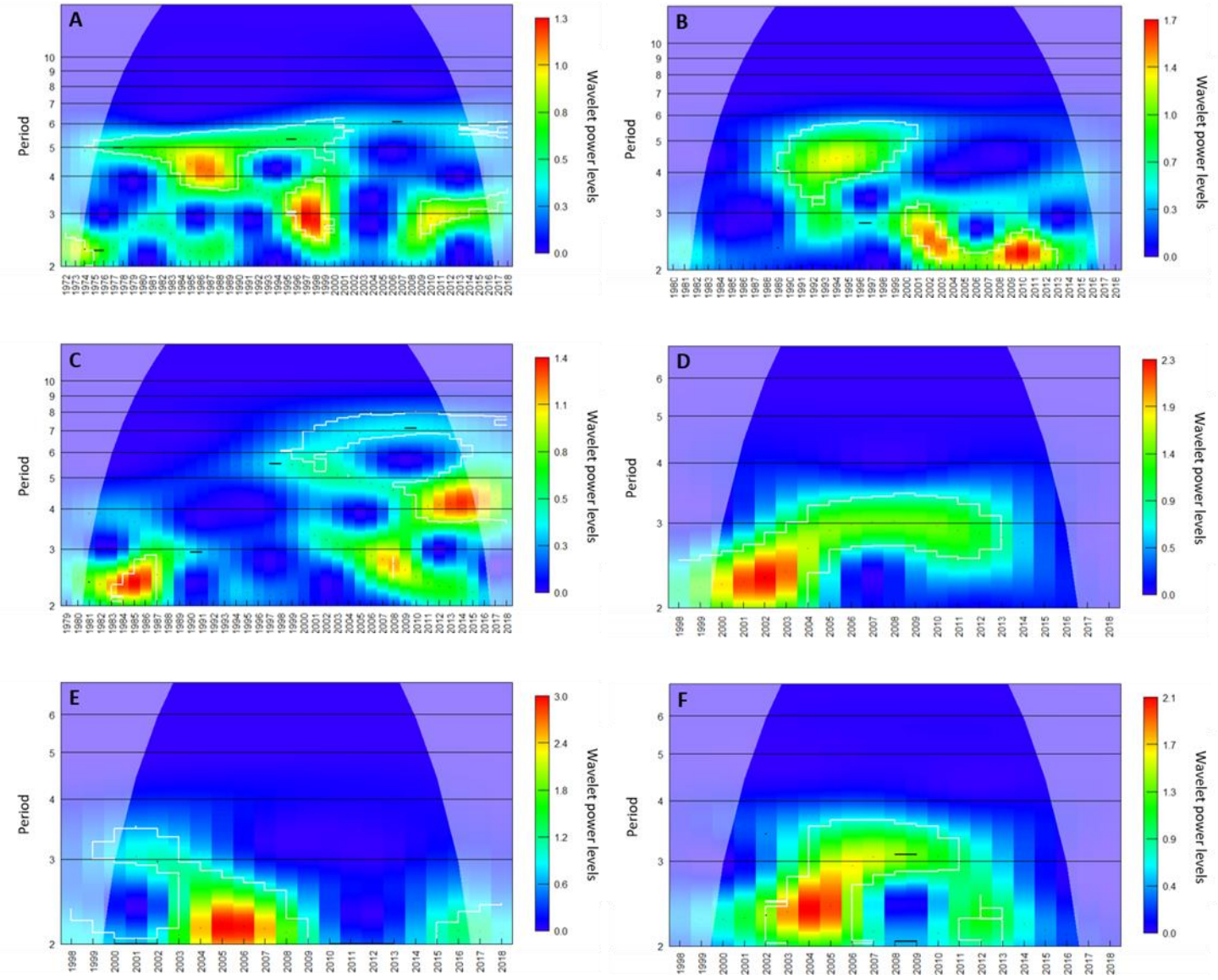

Figure A1 Wavelet power spectrum of the various environmental variables. Time series detrended using Local regression (LOESS; 30% smoothing span). The null hypothesis of "no periodicity" in these plots is tested with simulation algorithms. White contour lines delineate areas of significant periodicity ($p<0.1$). The shaded area indicates the cone of influence, which delimits the region not influenced by edge effects. **A)** Oceanic Nino Index (1972 – 2018) **B)** Antarctic Oscillation (1980 – 2018) **C)** September Antarctic sea ice extent (1979 – 2018) **D)** Mean January chlorophyll *a* concentration for postulated feeding ground A (1998 – 2018) **E)** Mean January chlorophyll *a* concentration for postulated feeding ground B (1998 – 2018) **F)** Mean January chlorophyll *a* concentration for postulated feeding ground C (1998 – 2018).

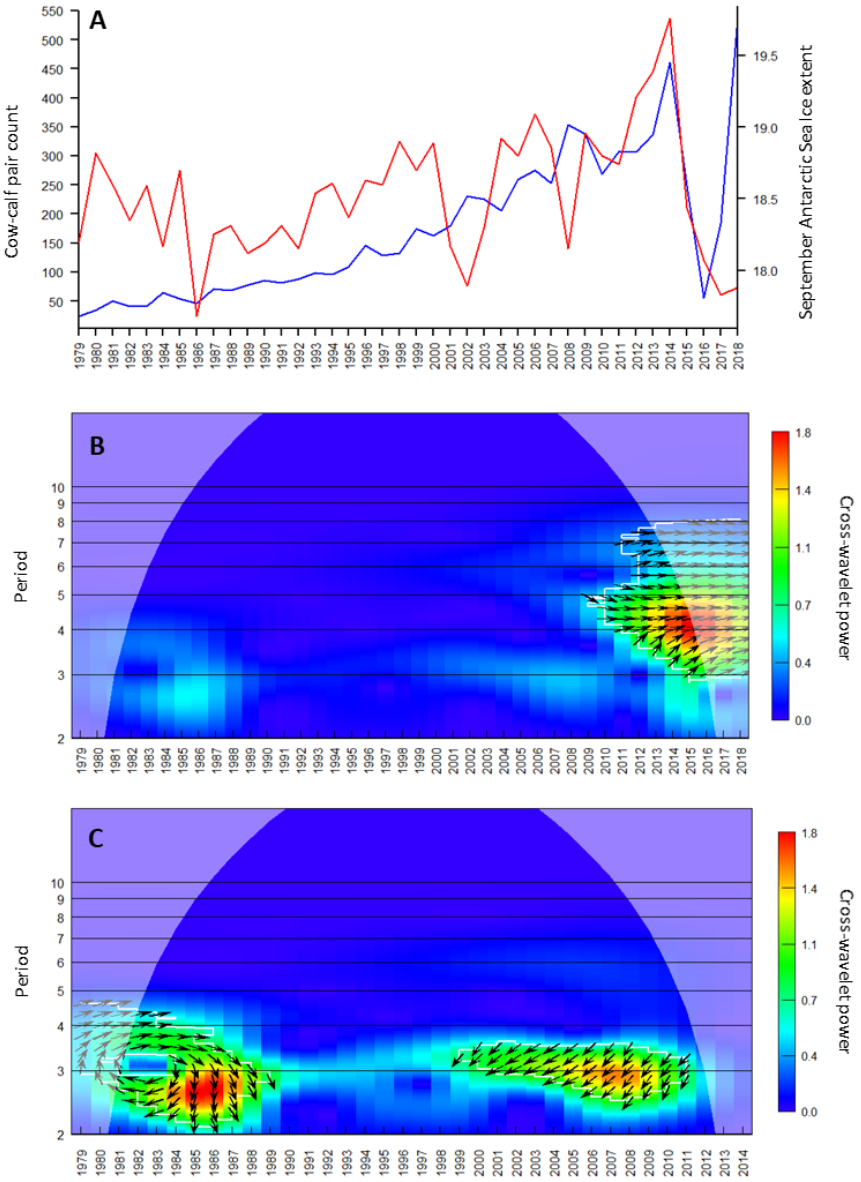

Figure A2 The association between log and detrended cow-calf pair counts, including and excluding the "crash" and the September Antarctic sea ice extent. **A)** Blue line: time series of southern right whale cow-calf pair counts, including the "crash" (1979 – 2018); red line: time series of the September Antarctic sea ice extent (1979 – 2018). **B)** Cross-wavelet power plot illustrating the synchrony in the cycles of southern right whale cow-calf pair counts including the "crash" (1979 – 2018) and the September Antarctic sea ice extent. **C)** Cross-wavelet power plot illustrating the synchrony in the cycles of southern right whale cow-calf pair counts excluding the "crash" (1979 – 2014) and the September Antarctic sea ice extent. Cross-wavelet power plots identify period bands and time intervals within which the cycles of the two time series are synchronised. The shaded area indicates the cone of influence, which delimits the region not influenced by edge effects. White contour lines border areas of significance. P-values associated with the values within the region delineated by the white contour lines are less than 5%.

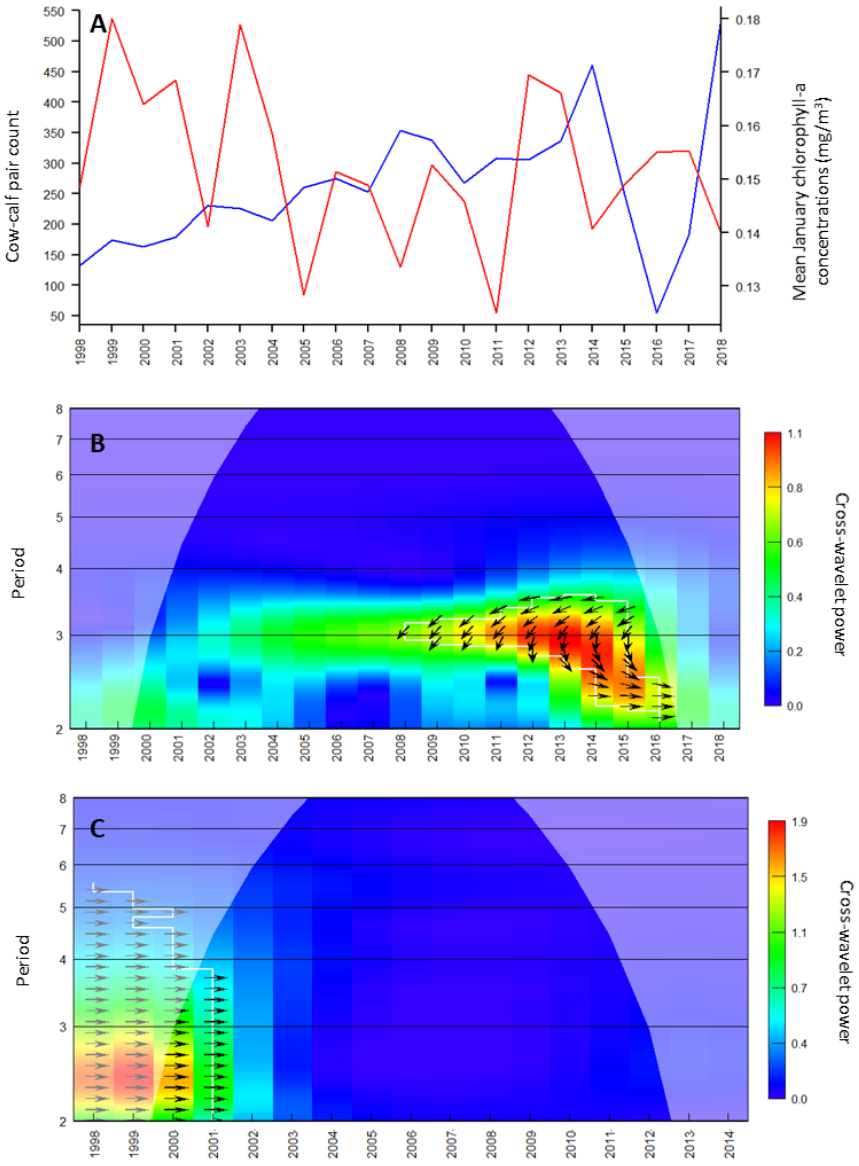

Figure A3 The association between log and detrended cow-calf pair counts, including and excluding the "crash" and the mean January chlorophyll *a* concentration for postulated feeding ground A. **A)** Blue line: time series of southern right whale cow-calf pair counts, including the "crash" (1998 – 2018); red line: time series of the mean January chlorophyll *a* concentration for postulated feeding ground A (1998 – 2018). **B)** Cross-wavelet power plot illustrating the synchrony in the cycles of southern right whale cow-calf pair counts including the "crash" (1998 – 2018) and the mean January chlorophyll *a* concentration for postulated feeding ground A. **C)** Cross-wavelet power plot illustrating the synchrony in the cycles of southern right whale cow-calf pair counts excluding the "crash" (1998 – 2014) and the mean January chlorophyll *a* concentration for postulated feeding ground A. Cross-wavelet power plots identify period bands and time intervals within which the cycles of the two time series are synchronised. The shaded area indicates the cone of influence, which delimits the region not influenced by edge effects. White contour lines border areas of significance. P-values associated with the values within the region delineated by the white contour lines are less than 5%.

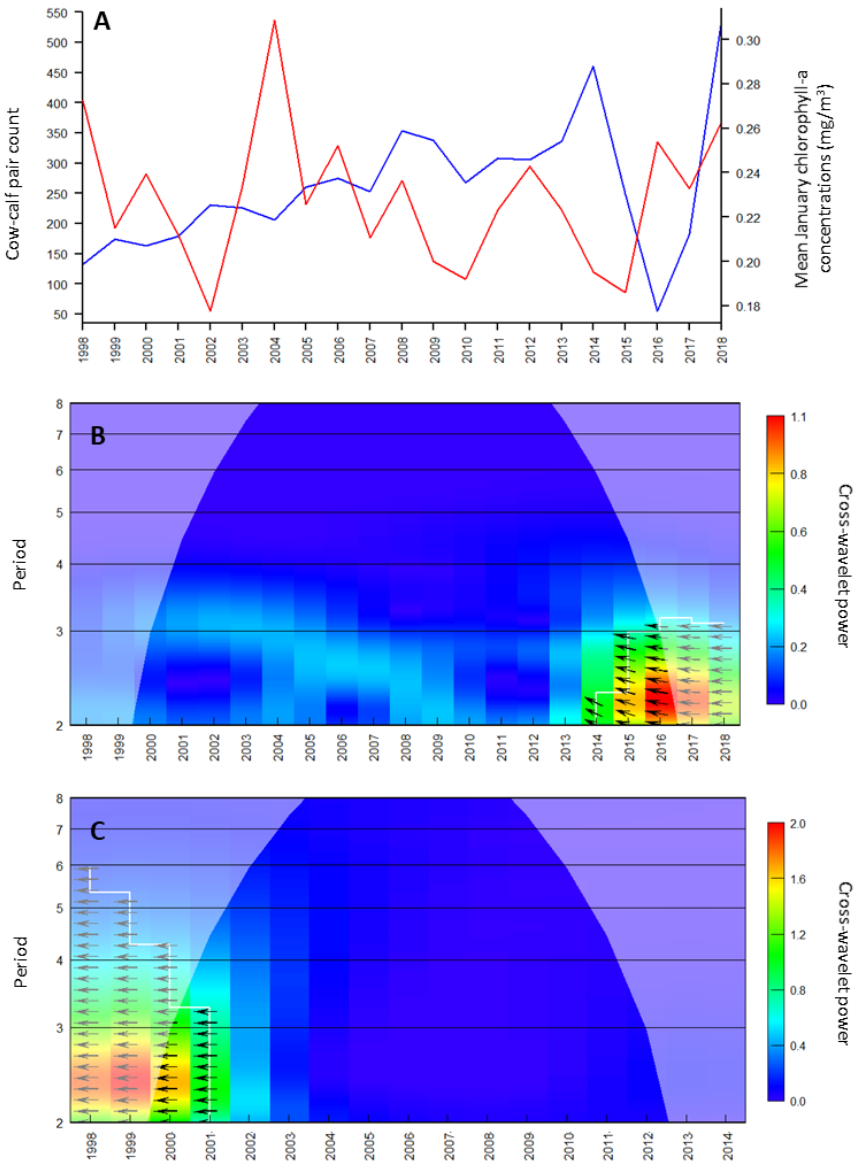

Figure A4 The association between log and detrended cow-calf pair counts, including and excluding the "crash" and the mean January chlorophyll *a* concentration for postulated feeding ground B. **A)** Blue line: time series of southern right whale cow-calf pair counts, including the "crash" (1998 – 2018); red line: time series of the mean January chlorophyll *a* concentration for postulated feeding ground B (1998 – 2018). **B)** Cross-wavelet power plot illustrating the synchrony in the cycles of southern right whale cow-calf pair counts including the "crash" (1998 – 2018) and the mean January chlorophyll *a* concentration for postulated feeding ground B. **C)** Cross-wavelet power plot illustrating the synchrony in the cycles of southern right whale cow-calf pair counts excluding the "crash" (1998 – 2014) and the mean January chlorophyll *a* concentration for postulated feeding ground B. Cross-wavelet power plots identify period bands and time intervals within which the cycles of the two time series are synchronised. The shaded area indicates the cone of influence, which delimits the region not influenced by edge effects. White contour lines border areas of significance. P-values associated with the values within the region delineated by the white contour lines are less than 5%.

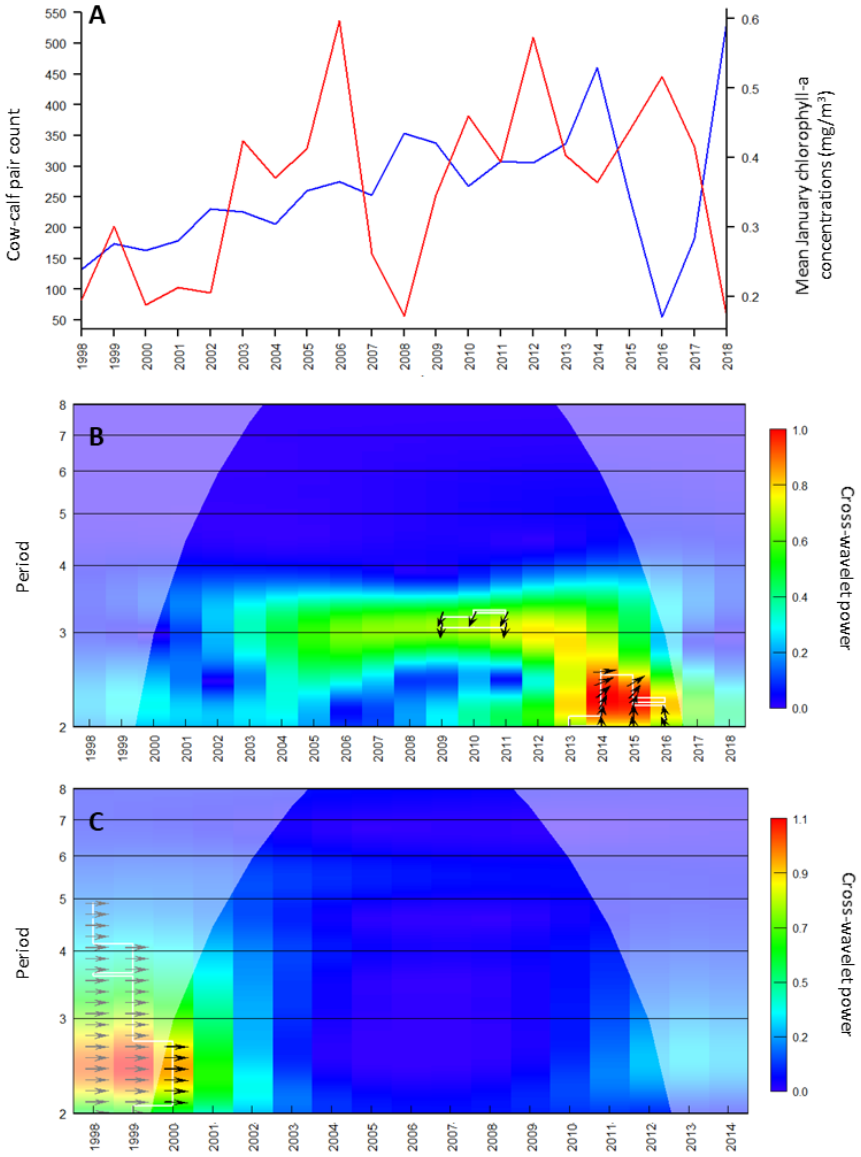

Figure A5 The association between log and detrended cow-calf pair counts, including and excluding the "crash" and the mean January chlorophyll *a* concentration for postulated feeding ground C. **A)** Blue line: time series of southern right whale cow-calf pair counts, including the "crash" (1998 – 2018); red line: time series of the mean January chlorophyll *a* concentration for postulated feeding ground C (1998 – 2018). **B)** Cross-wavelet power plot illustrating the synchrony in the cycles of southern right whale cow-calf pair counts including the "crash" (1998 – 2018) and the mean January chlorophyll *a* concentration for postulated feeding ground C. **C)** Cross-wavelet power plot illustrating the synchrony in the cycles of southern right whale cow-calf pair counts excluding the "crash" (1998 – 2014) and the mean January chlorophyll *a* concentration for postulated feeding ground A. Cross-wavelet power plots identify period bands and time intervals within which the cycles of the two time series are synchronised. The shaded area indicates the cone of influence, which delimits the region not influenced by edge effects. White contour lines border areas of significance. P-values associated with the values within the region delineated by the white contour lines are less than 5%.

Table A1 ARIMA model results for the first lag incorporation method. Models 1-10: third class of ARIMA models: growth rate anomalies and the ONI, AAO and SASIE; excluding the "crash". Models 11-19: fourth class of ARIMA models: growth rate anomalies and chlorophyll *a* concentrations from postulated feeding ground A, B and C; excluding the "crash". Significant model performance improvement compared to the original model (excluding predictors) is indicated via * (0.1 significance level) and ** (0.05 significance level).

Model number	Length of Data	Model Order / Predictors	Log Likelihood	AIC	Adjusted R^2
1	1982-2014	(3, 2, 6)	41.38	-62.76	0.7779
2	1982-2014	(3, 2, 6) / ONI*(t)*	41.77	-61.53	0.7815
3	1982-2014	(3, 2, 6) / ONI*(t)* + ONI*(t-1)*	42.74	-61.49	0.8171
4	1982-2014	(3, 2, 6) / ONI*(t)* + ONI*(t-1)* + ONI*(t-2)*	43.33	-60.67	0.8059
5	1982-2014	(3, 2, 6) / AAO*(t)*	43.31	-64.61	0.8266
6	1982-2014	(3, 2, 6) / AAO*(t)* + AAO*(t-1)*	43.61	-63.21	0.8295
7	1982-2014	(3, 2, 6) / AAO*(t)* + AAO*(t-1)* + AAO*(t-2)*	43.61	-61.22	0.8298
8	1982-2014	(3, 2, 6) / SASIE*(t)*	41.39	-60.78	0.7787
9	1982-2014	(3, 2, 6) / SASIE*(t)* + SASIE*(t-1)*	41.61	-59.23	0.7812
10	1982-2014	(3, 2, 6) / SASIE*(t)* + SASIE*(t-1)* + SASIE*(t-2)*	42.29	-58.57	0.7892
11	2000-2014	(4, 0, 0)	17.66	-23.31	0.7005
12	2000-2014	(4, 0, 0) / Ground A*(t)*	18.25	-22.5	0.7408
13	2000-2014	(4, 0, 0) / Ground A*(t)* + Ground A*(t-1)*	18.53	-21.07	0.7637
14	2000-2014	(4, 0, 0) / Ground A*(t)* + Ground A*(t-1)* + Ground A*(t-2)*	23.29	-28.57	0.8475
15	2000-2014	(4, 0, 0) / Ground B*(t)*	18.21	-22.42	0.7198
16	2000-2014	(4, 0, 0) / Ground B*(t)* + Ground B*(t-1)*	18.3	-20.61	0.7179
17	2000-2014	(4, 0, 0) / Ground B*(t)* + Ground B*(t-1)* + Ground B*(t-2)*	22.14	-26.28	0.8420
18	2000-2014	(4, 0, 0) / Ground C*(t)*	18.25	-22.5	0.7408
19	2000-2014	(4, 0, 0) / Ground C*(t)* + Ground C*(t-1)*	18.53	-21.07	0.7637

Table A2 ARIMA model results for the second lag incorporation method. Models 1-23: third class of ARIMA models: growth rate anomalies and the ONI, AAO and SASIE; excluding the "crash". Significant model performance improvement compared to the original model (excluding predictors) is indicated via * (0.1 significance level) and ** (0.05 significance level).

Model number	Length of Data	Model Order / Predictors	Log Likelihood	AIC	Adjusted R^2
1	1982-2014	(3, 2, 6)	41.38	-62.76	0.7779
20	1982-2014	(3, 2, 6) / ONI*(t)* + ONI*(t-1)* + ONI*(t-2)* + AAO(t) + AAO(t-1) + AAO(t-2) + SASIE(t) + SASIE(t-1) + SASIE(t-2)	47.74	-57.49	0.8709
21	1982-2014	(3, 2, 6) / ONI*(t)* + ONI*(t-1)* + ONI*(t-2)* + AAO(t) + AAO(t-1) + AAO(t-2)	44.38	-56.77	0.8373
22	1982-2014	(3, 2, 6) / ONI*(t)* + ONI*(t-1)* + ONI*(t-2)* + SASIE(t) + SASIE(t-1) + SASIE(t-2)	39.55	-47.1	0.7668
23	1982-2014	(3, 2, 6) / AAO(t) + AAO(t-1) + AAO(t-2) + SASIE(t) + SASIE(t-1) + SASIE(t-2)	45.82	-59.64	0.8553

References

Atkinson A, Siegel V, Pakhomov E, Rothery P (2004) Long-term decline in krill stock and increase in salps within the Southern Ocean. Nature 432:100–103

Atkinson A, Siegel V, Pakhomov EA, Rothery P, Loeb V, Ross RM, Quetin LB, Schmidt K, Fretwell P, Murphy EJ, Tarling GA, Fleming AH (2008) Oceanic circumpolar habitats of Antarctic krill. Mar Ecol Prog Ser 362:1–23

Barbosa A, Benzal J, León A de, Moreno J (2012) Population decline of chinstrap penguins (*Pygoscelis antarctica*) on Deception Island, South Shetlands, Antarctica. Polar Biol 35:1453–1457

Best P, Brandão A, Butterworth D (2001) Demographic parameters of southern right whales off South Africa. J Cetacean Res Manage (Special Issue) 2:161–169

Best P, Brandão A, Butterworth D (2010) Estimates of Demographic Parameters for Southern Right Whales. Int Whal Comm:1–17

Best P, Folkens PA (2007) Whales and dolphins of the southern African subregion. Cambridge University Press

Best P, Schell D (1996) Stable isotopes in southern right whale (*Eubalaena australis*) baleen as indicators of seasonal movements, feeding and growth. Mar Biol 124:483–494

Braithwaite JE, Meeuwig JJ, Letessier TB, Jenner KCS, Brierley AS (2015) From sea ice to blubber: linking whale condition to krill abundance using historical whaling records. Polar Biol 38:1195–1202

Brandão A, Best P, Butterworth D (2011) Monitoring the recovery of the southern right whale in South African waters. IWC Doc SC S 11

Brandão A, Vermeulen E, Ross-Gillespies A, Findlay K, Butterworth DS (2018) Updated application of a photo-identification based assessment model to southern right whales in South African waters, focussing on inferences to be drawn from a series of appreciably lower counts of calving females over 2015 to 2017. Report presented at the 67th IWC scientific committee

Brodie PF (1975) Cetacean energetics, an overview of intraspecific size variation. Ecology 56:152–161

Bunker AJ, Hirst AG (2004) Growth of marine planktonic copepods: Global rates and patterns in relation to chlorophyll *a*, temperature and body weight. Mar Ecol Prog Ser 279:161–181

Cai W (2006) Antarctic ozone depletion causes an intensification of the Southern Ocean super-gyre circulation. Geophys Res Lett 33:1–4

Carroll EL, Baker CS, Watson M, Alderman R, Bannister J, Gaggiotti OE, Gröcke DR, Patenaude N, Harcourt R (2015) Cultural traditions across a migratory network shape the genetic structure of southern right whales around Australia and New Zealand. Sci Rep 5:1–12

Cazelles B, Chavez M, Berteaux D, Ménard F, Vik J, Jenouvrier S, Stenseth N (2008) Wavelet analysis of ecological time series. Oecologia 156:287–304

Chen L, Li T, Wang B, Wang L (2017) Formation Mechanism for 2015/16 Super El Niño. Sci Rep 7:1–10

Constable AJ, Melbourne-Thomas J, Corney SP, Arrigo KR, Barbraud C, Barnes DKA, Bindoff NL, Boyd PW, Brandt A, Costa DP, Davidson AT, Ducklow HW, Emmerson L, Fukuchi M, Gutt J, Hindell MA, Hofmann EE, Hosie GW, Iida T, Jacob S, Johnston NM, Kawaguchi S, Kokubun N, Koubbi P, Lea M-A, Makhado A, Massom RA, Meiners K, Meredith MP, Murphy EJ, Nicol S, Reid K, Richerson K, Riddle MJ, Rintoul SR, Smith WO, Southwell C, Stark JS, Sumner M, Swadling KM, Takahashi KT, Trathan PN, Welsford DC, Weimerskirch H, Westwood KJ, Wienecke BC, Wolf-Gladrow D, Wright SW, Xavier JC, Ziegler P (2014) Climate change and Southern Ocean ecosystems I: how changes in physical habitats directly affect marine biota. Glob Chang Biol 20:3004–3025

Corkeron J, Connor C (1999) Why do baleen whales migrate? Mar Mammal Sci 15:1228–1245

Croxall JP, Reid K, Prince PA (1999) Diet, provisioning and productivity responses of marine predators to differences in avaiability ofr Antarctic krill. Mar Ecol Progr Ser 177:115–131

Duxbury AC, Duxbury AB, Sverdrup K (1999) an introduction to the World's Oceans. McGraw-Hill, Boston

Elwen S, Best P (2004) Environmental factors influencing the distribution of southern right whales (*Eubalaena australis*) on the south coast of South Africa II: Within bay distribution. Mar Mammal Sci 20:583–601

Evans PG (1987) The natural history of whales & dolphins. Academic Press Inc

Flores H, Atkinson A, Kawaguchi S, Krafft BA, Milinevsky G, Nicol S, Reiss C, Tarling GA, Werner R, Bravo Rebolledo E, Cirelli V, Cuzin-Roudy J, Fielding S, Groeneveld JJ, Haraldsson M, Lombana A, Marschoff E, Meyer B, Pakhomov EA, Rombolá E, Schmidt K, Siegel V, Teschke M, Tonkes H, Toullec JY, Trathan PN, Tremblay N, Putte AP Van De, Franeker JA Van, Werner T (2012) Impact of climate change on Antarctic krill. Mar Ecol Prog Ser 458:1–19

Forcada J, Trathan PN, Reid K, Murphy EJ (2005) The effects of global climate variability in pup production of antarctic fur seals. Ecology 86:2408–2417

Fraser W., Hofmann E. (2003) A predator's perspective on causal links between climate change, physical forcing and ecosystem response. Mar Ecol Prog Ser 265:1–15

Greene C, Pershing A (2004) North Atlantic right whales: the right whale at the wrong time ? Front Ecol Environ 2:29–34

Greene CH, Pershing AJ, Kenney RD, Jossi JW (2003) Impact of Climate Variability on the Recovery of Endangered North Atlantic Right Whales. Oceanography 16:98–103

Hlista BL, Sosik HM, Traykovski LVM, Kenney RD, Moore MJ (2009) Seasonal and interannual correlations between right-whale distribution and calving success and chlorophyll concentrations in the Gulf of Maine, USA. Mar Ecol Prog Ser 394:289–302

Holmgren M, Scheffer M, Ezcurra E, Gutiérrez JR, Mohren GMJ (2001) El Niño effects on the dynamics of terrestrial ecosystems. Trends Ecol Evol 16:89–94

Hyndman R, Athanasopoulos G, Bergmeir C, Caceres G, Chhay L, O'Hara-Wild M, Petropoulos F, Razbash S, Wang E, Yasmeen F (2019) forecast: Forecasting functions for time series and linear models. R package version 8.5

International Whaling Commission (IWC) (2013) Report of the IWC workshop on the assessment of southern right whales. J. Cetacean Res. Manage.14 (Suppl.): 439-462.

Jenouvrier S, Caswell H, Barbraud C, Holland M, Strœve J, Weimerskirch H (2009) Demographic models and IPCC climate projections predict the decline of an emperor penguin population. Proc Natl Acad Sci 106:1844–1847

Kiørboe T, Nielsen T (1994) Regulation of zooplankton biomass and production coastal ecosystem.1 . Copepods. Limnol Oceanogr 39:493–507

Leaper R, Cooke J, Trathan P, Reid K, Rowntree V, Payne R (2006) Global climate drives southern right whale (*Eubalaena australis*) population dynamics. Biol Lett 2:289–292

Liu J, Yuan X, Rind D, Martinson DG (2002) Mechanism study of the ENSO and southern high latitude climate teleconnections. Geophys Res Lett 29:24-1-24–4

Lockyer C (1986) Body Fat Condition in Northeast Atlantic Fin Whales, *Balaenoptera physalus* , and Its Relationship with Reproduction and Food Resource. Can J Fish Aquat Sci 43:142–147

Loeb VJ, Hofmann EE, Klinck JM, Holm-Hansen O, White WB (2009) ENSO and variability of the antarctic peninsula pelagic marine ecosystem. Antarct Sci 21:135–148

Loeb VJ, Santora JA (2015) Climate variability and spatiotemporal dynamics of five Southern Ocean krill species. Prog Oceanogr 134:93–122

Loeb V, Siegel V, Holm-Hansen O, Hewitt R, Fraser W, Trivelpiece W, Trivelpiece S (1997) Effects of sea-ice extend and krill or salp dominance on the Antartic food web. Nature 387.:897–900

Lovenduski NS, Gruber N (2005) Impact of the Southern Annular Mode on Southern Ocean circulation and biology. Geophys Res Lett 32:1–4

Murphy EJ, Trathan PN, Watkins JL, Reid K, Meredith MP, Forcada J, Thorpe SE, Johnston NM, Rothery P (2007) Climatically driven fluctuations in Southern Ocean ecosystems. Proc R Soc B Biol Sci 274:3057–3067

Nicol S, Worby A, Leaper R (2008) Changes in the Antarctic sea ice ecosystem: Potential effects on krill and baleen whales. Mar Freshw Res 59:361–382

NMFS (2007) Southern right whale (*Eubalaena australis*) 5-year review: summary and evaluation. Natl Mar Fish Serv

Norris KS (1967) Some observations on the migration and orientation of marine mammals. In: Storm R.M, editor. Animal orientation and migration. Oregon State University Press; Corvallis 101–125

Patenaude NJ, Portway VA, Schaeff CM, Bannister JL, Best P, Payne RS, Rowntree VJ, Rivarola M, Baker CS (2007) Mitochondrial DNA diversity and population structure among southern right whales (*Eubalaena australis*). J Hered 98:147–157

Pohl B, Fauchereau N, Reason CJC, Rouault M (2010) Relationships between the Antarctic oscillation, the Madden-Julian oscillation, and ENSO, and consequences for rainfall analysis. J Clim 23:238–254

QGIS Development Team (2009) QGIS Geographic Information System. Open Source Geospatial Foundation. URL http://qgis.org

R Core Team (2018). R: A language and environment for statistical computing. R Foundation for Statistical Computing, Vienna, Austria. URL http://www.R-project.org/

Reeves R, Rolland R, Clapham P (2000) Causes of reproductive failure in North Atlantic right whales: new avenues of research. Report of a Workshop held 26-28 April 2000, Falmouth, MA NEFSC 1–46

Reilly SB, Bannister JL, Best P, Brown M, Jr. B, R.L., Butterworth D, Clapham PJ, Cooke J, Donovan GP, Urbán J, Zerbini AN (2013) *Eubalaena australis*, Southern Right Whale View. IUCN Red List Threat Species

Rosch A, Schmidbauer H (2018) WaveletComp: Computational Wavelet Analysis. R package version 1.1, 1–38

Salinger J, Hobday AJ, Matear RJ, O'Kane TJ, Risbey JS, Dunstan P, Eveson JP, Fulton EA, Feng M, Plagányi E, Poloczanska ES, Marshall AG, Thompson PA (2016) Decadal-Scale Forecasting of Climate Drivers for Marine Applications. Adv Mar Biol 74:1–68

Seyboth E, Groch KR, Dalla Rosa L, Reid K, Flores PAC, Secchi ER (2016) Southern Right Whale (Eubalaena australis) Reproductive Success is Influenced by Krill (*Euphausia superba*) Density and Climate. Sci Rep 6

Shreeve RS, Ward P, Whitehouse MJ (2002) Copepod growth and development around South Georgia: Relationships with temperature, food and krill. Mar Ecol Prog Ser 233:169–183

Tormosov DD, Mikhaliev YA, Best P, Zemsky VA, Sekiguchi K, Brownell RL (1998) Soviet catches of southern right whales Eubalaena australis, 1951-1971. Biological data and conservation implications. Biol Conserv 86:185–197

Townsend CH (1935) The distribution of certain whales as shown by logbook records of American whaleships. Zoologica 19:1–50

Trathan PN, Brierley AS, Brandon MA, Bone DG, Goss C, Grant SA, Murphy EJ, Watkins JL (2003) Oceanographic variability and changes in Antarctic krill (*Euphausia superba*) abundance at South Georgia. Fish Oceanogr 12:569–583

Trathan PN, Forcada J, Murphy EJ (2007) Environmental forcing and Southern Ocean marine predator populations: effects of climate change and variability. Philos Trans R Soc Biol Sci:2351–2365

Trathan PN, Fretwell PT, Stonehouse B (2011) First recorded loss of an emperor penguin colony in the recent period of Antarctic regional warming: Implications for other colonies. PLoS One 6

Trathan PN, Ratcliffe N, Masden EA (2012) Ecological drivers of change at South Georgia: The krill surplus, or climate variability. Ecography 35:983–993

Trapletti A, Hornik K (2018) tseries: Time Series Analysis and Computational Finance. R package version 0.10-46

Turner J (2004) The El Niño-Southern Oscillation and Antarctica. Int J Climatol 24:1–31

Valenzuela LO, Sironi M, Rowntree VJ, Sala L La, Pozzi L, Mohamed N, Musmeci L, Andrejuk J, Uhart M, Chirife A, Maron C (2008) Population genetic structure of living and dead southern right whales (*Eubalaena australis*) off Península Valdés, Argentina. Cetac Res Manag 62:1–12

Valenzuela LO, Sironi M, Rowntree VJ, Seger J (2009) Isotopic and genetic evidence for culturally inherited site fidelity to feeding grounds in southern right whales (*Eubalaena australis*). Mol Ecol 18:782–791

Vermeulen E, Wilkinson C, Thornton M, Peters IT, Findlay, K (2018) Report on the 2017 Mammal Research Institute Whale Unit Southern Right Whale Survey, Nature's Valley to Lamberts Bay, South Africa. Report presented to the 67th IWC scientific committee

Ward EJ, Holmes EE, Balcomb KC (2009) Quantifying the effects of prey abundance on killer whale reproduction. J Appl Ecol 46:632–640

Williams R, Vikingsson GA, Gislason A, Lockyer C, New L, Thomas L, Hammond PS (2013) Evidence for density-dependent changes in body condition and pregnancy rate of North Atlantic fin whales over four decades of varying environmental conditions. ICES J Mar Sci 70:1273–1280